nature biomedical engineering

Article

https://doi.org/10.1038/s41551-025-01478-6

A modular vaccine platform for optimized lipid nanoparticle mRNA immunogenicity

Received: 20 December 2023

Accepted: 30 June 2025

Published online: 25 August 2025

Check for updates

Zhenhao Fang[1,2,3,14], Valter S. Monteiro[4,14], Changin Oh[1], Kawthar Al Janabi[1,2,3,5], Luciano Romero[1,2,3,5], Nabihah Ahsan[1,2,3,5], Luojia Yang[1,2,3,6], Lei Peng[1,2,3], Daniel DiMaio[1,7,8,9], Carolina Lucas[4,10,11,15] & Sidi Chen[1,2,3,4,5,6,9,12,13,15]

Certain messenger RNA antigens in mRNA vaccines elicit an insufficient immune response due to challenges in cell surface translocation (CST) of the antigens. Here we develop a modular vaccine platform (MVP) to enhance the immunogenicity of challenging mRNA antigens by optimizing antigen expression and presentation. MVPs enable the modular assembly of chimeric antigens. Our platform comprises diverse modules capable of generating >2,500 combinations with any antigen and displaying distinct antigen epitopes on the cell surface. We quantify the CST efficacy of various modules using multiple antigens, including the mpox virus (MPXV) proteins A29, M1R and A35R, and compare chimeric antigen surface expression in multiple cell lines. Using MPXV as a model, we identify optimal modules that enhance the CST of multiple MPXV antigens, improving the immune response of lipid nanoparticle mRNAs and protecting against lethal viral challenge. With these effective CST modules, we further demonstrate the generalizability of MVP by optimizing additional mRNA antigens, including the human papillomavirus 16 proteins E6 and E7 and the varicella zoster virus glycoprotein gE. This platform is applicable to any antigen of interest, facilitating the development of mRNA vaccines against challenging targets.

Messenger RNA vaccine technology has gained attention for its use against various diseases and pathogens, including severe acute respiratory syndrome coronavirus 2 (SARS-CoV-2) variants, human metapneumovirus[1], cytomegalovirus[2], Epstein–Barr virus, herpes simplex virus[3], human papillomavirus (HPV)[4], human immunodeficiency virus[5], mpox virus (MPXV; formally known as monkeypox virus)[6], varicella zoster virus (VZV)[7], norovirus, Zika virus[8], malaria, Lyme disease and cancer[9]. Using an antigen encoded in the mRNA sequence accelerates manufacturing and reduces costs compared with recombinant protein and attenuated or inactivated virus vaccines[10].

Traditional vaccines deliver antigens directly to the extracellular space, whereas mRNA vaccine antigens are expressed inside the recipient's cells and rely on additional mechanisms to translocate to the extracellular space. The translocation of these antigens to the extracellular space may pose potential challenges for mRNA vaccines expressing certain types of antigens. Many viral antigens translocate

[1]Department of Genetics, Yale University School of Medicine, New Haven, CT, USA. [2]Systems Biology Institute, Yale University, West Haven, CT, USA. [3]Center for Cancer Systems Biology, Yale University, West Haven, CT, USA. [4]Immunobiology Program, Yale University, New Haven, CT, USA. [5]Yale College, New Haven, CT, USA. [6]Molecular Cell Biology, Genetics, and Development Program, Yale University, New Haven, CT, USA. [7]Department of Therapeutic Radiology, Yale School of Medicine, New Haven, CT, USA. [8]Department of Molecular Biophysics and Biochemistry, Yale University, New Haven, CT, USA. [9]Yale Cancer Center, Yale University School of Medicine, New Haven, CT, USA. [10]Center for Infection and Immunity, Yale University, New Haven, CT, USA. [11]Department of Immunobiology, Yale University School of Medicine, New Haven, CT, USA. [12]Stem Cell Center, Yale University School of Medicine, New Haven, CT, USA. [13]Center for Biomedical Data Science, Yale University School of Medicine, New Haven, CT, USA. [14]These authors contributed equally: Zhenhao Fang, Valter S. Monteiro. [15]These authors jointly supervised this work: Carolina Lucas, Sidi Chen. e-mail: Carolina.lucas@yale.edu; sidi.chen@yale.edu

to the extracellular space by forming protein complexes on viral particles[11]. For example, the MPXV antigen A29 (or A29L) is a surface antigen on the viral envelope and a well-characterized target of neutralizing antibodies[12,13]. Immunization with the MPXV A29 protein in vivo has been reported to elicit a substantial neutralizing antibody response[14]. However, vaccination with A29 lipid nanoparticle (LNP) mRNA led to a poor antibody response[6,15]. Further analysis of the A29 sequence and subcellular localization revealed that its sequence lacks a membrane translocation signal, causing it to be retained in the cytosol when expressed alone[6], suggesting that its surface translocation relies on co-localization with other viral proteins.

Additionally, a recent study indicated that synthetic peptides of 27-base polymer/oligonucleotide neoepitopes from B16F10 tumour cells were more likely to trigger T cell responses than mRNAs encoding the same neoantigens[16], possibly due to a lack of translocation of the mRNAs. The native sequences of these antigens lack potent signals for translocation to the extracellular space, making it difficult for B cells and antigen-presenting cells (APCs) to recognize these intracellular antigens. Many vaccine targets resemble MPXV A29 or B16F10 neoantigens, such as the protein encoded by mutated *KRAS*[9], the proteins HPV E7 (ref. 17), HPV L1 (ref. 18) and norovirus VP1 (ref. 19), the Lyme disease antigen OspA[20], and the malaria antigen Pfs25 (ref. 21).

Additionally, insufficient extracellular translocation of mRNA antigens may lead to poor immunogenicity, as isolated expression of selected surface antigens from the viral proteome can weaken their translocation signals. Viruses such as herpes simplex virus, VZV, Epstein–Barr virus, MPXV and cytomegalovirus have genomes ranging from 100–300 kilobases in length and encode approximately 100–200 proteins, whereas some other viral pathogens are much smaller. In contrast, pathogens causing Lyme disease, malaria and tuberculosis have genomes comprising between 1 and 30 megabases, encoding thousands of proteins. The glycoproteins of these pathogens exist within a network of protein complexes, and a single antigen may not possess cell surface translocation (CST) signals as potent as those of the SARS-CoV-2 spike protein, for which CST solely relies on its own sorting signals. Improving CST signals for these mRNA antigens becomes a crucial challenge in the development of effective mRNA vaccines against these pathogens.

Cellular factors such as antigen subcellular localization, surface expression, oligomerization, secretion and mRNA translation are crucial for successful induction of effective immune responses. To optimize these factors, we built a modular vaccine platform (MVP) for optimized LNP mRNA immunogenicity by engineering these elements using an unbiased and rational design method. In this study, we investigated whether enhancing an mRNA antigen's CST would improve its immune response. We also determined the signals that translocate membrane proteins or antigens of interest to the cell surface and whether these CST signals can be grafted onto mRNA antigens to increase their surface expression. In this Article, we look at how these signals alter immune responses to chimeric antigens, the relationship between antigen surface expression, antibody response and T cell response, how to evaluate the antigen surface translocation strength of different CST modules and whether the signal strengths of CST modules change when they translocate different antigens to the cell surface. We use the MVP, along with flow cytometry, enzyme-linked immunosorbent assay (ELISA), T cell functional assays and viral challenge experiments, to comprehensively explore and optimize the surface expression levels, antibody response, T cell response and overall protection efficacy of mRNA antigens following mRNA vaccination.

Results

The MVP enhances the immune response of mpox mRNA antigens in mice

We initiated our investigation by testing the optimal engineering of effective LNP mRNA antigens with different modules. To determine whether the immune response to mRNA antigens can be enhanced by modifying their CST sequences, we created libraries of multiple CST modules from single-pass transmembrane proteins on the cell membrane. We established the MVP to recombine antigen ectodomains with CST modules and characterized the CST levels and immunogenicity of these chimeric antigens in vivo (Fig. 1a). By systematically evaluating the effect of these modifications, we aimed to optimize the expression and immune response of mpox mRNA antigens in mice, thereby demonstrating the potential of the MVP platform to enhance mRNA vaccine efficacy.

To identify CST sequences, we first analysed transmembrane proteins using plasma membrane localization records in the Human Proteome Atlas. We extracted their domain boundaries, secondary structure, hydrophobicity, isoelectric point, protein sequence, size, membrane topology and cellular localization information (Methods and Supplementary Tables 1 and 2). The identified CST sequences were then grouped based on membrane topology into type I (amino (N) terminus in the extracellular space) and type II sequences (N terminus in the cytosol), which were further separated into several modules, including signal peptide (SP), extracellular hinge plus transmembrane domain (TM) and cytosolic segments (C). The parental vector we used contains untranslated region (UTR), green fluorescent protein (GFP) and type IIS digestion sites to enable dropout selection and rapid one-pot assembly. Importantly, the MPXV antigens in this study were used as model antigens, comprising three major categories of mRNA antigens: type I/III (N-terminal ectodomain; E8L, M1R and B6R), type II (C-terminal ectodomain; A35R) and soluble antigens (A29).

Using a series of constructs, we established a one-stop platform to optimize type I, type II and soluble mRNA antigens. Of note, the SARS-CoV-2 spike protein, successfully targeted by the first Food and Drug Administration-approved LNP mRNA vaccines[22,23], served as a benchmark antigen that is known to induce high antibody titres. Additionally, MPXVac-097, expressing five MPXV antigens (A29, A35R, E8L, M1R and B6R) developed in our previous study, was used as a model to compare with the benchmark spike LNP mRNA[6]. Mice were immunized on days 0, 14 and 28. Antibody titres in mouse plasma were assessed at baseline, day 28 and day 33 (Fig. 1b). Before immunization (day 0), antibody titres were at baseline levels (Supplementary Figs. 1 and 2). Antibody titre plateaus (area under the curve (AUC) = ~3) were observed after two doses of spike wild type on day 28 and three doses of MPXVac-097 on day 33 (Fig. 1c), indicating that mpox mRNA antigens have additional optimization space to reach immunogenicity comparable to spike. Consistent with previous reports[6,24], immunization with spike or MPXVac-097 elicited potent antibody responses to spike, E8 and A35 proteins. Co-immunization with spike and MPXVac-097 induced similar levels of antibody response compared with individual immunizations (Fig. 1b,c and Supplementary Figs. 1b and 3a–c), supporting the feasibility of concurrent immunizations.

To evaluate the efficacy of MVP modules, we first tested whether SPs fused to the N terminus of the antigen can enhance the antibody response of MPXV antigens. Mice were immunized with MPXV antigen LNP mRNAs with or without tissue plasminogen activator (tPA) SP (Fig. 1d and Supplementary Fig. 4). After two immunizations, tPA SP significantly increased antibody responses to E8L and A29 antigens. Notably, the [tPA SP]–E8L antibody titre reached an AUC of 3 (square brackets represent MVP modules). These data suggested that tPA SP can significantly enhance the immunogenicity of certain MPVX antigens, such as E8L and A29, thereby optimizing the effectiveness of mRNA vaccines for these challenging antigens.

Effects of UTR and nucleotide composition on mRNA antigens

Because of the observed improvement induced by tPA SP, we sought to further optimize the mRNA antigen design using other modules, such as UTR sequences and type I and II transmembrane and cytosolic (TM/C) domains. UTR sequences play a critical role in mRNA stability

https://doi.org/10.1038/s41551-025-01478-6

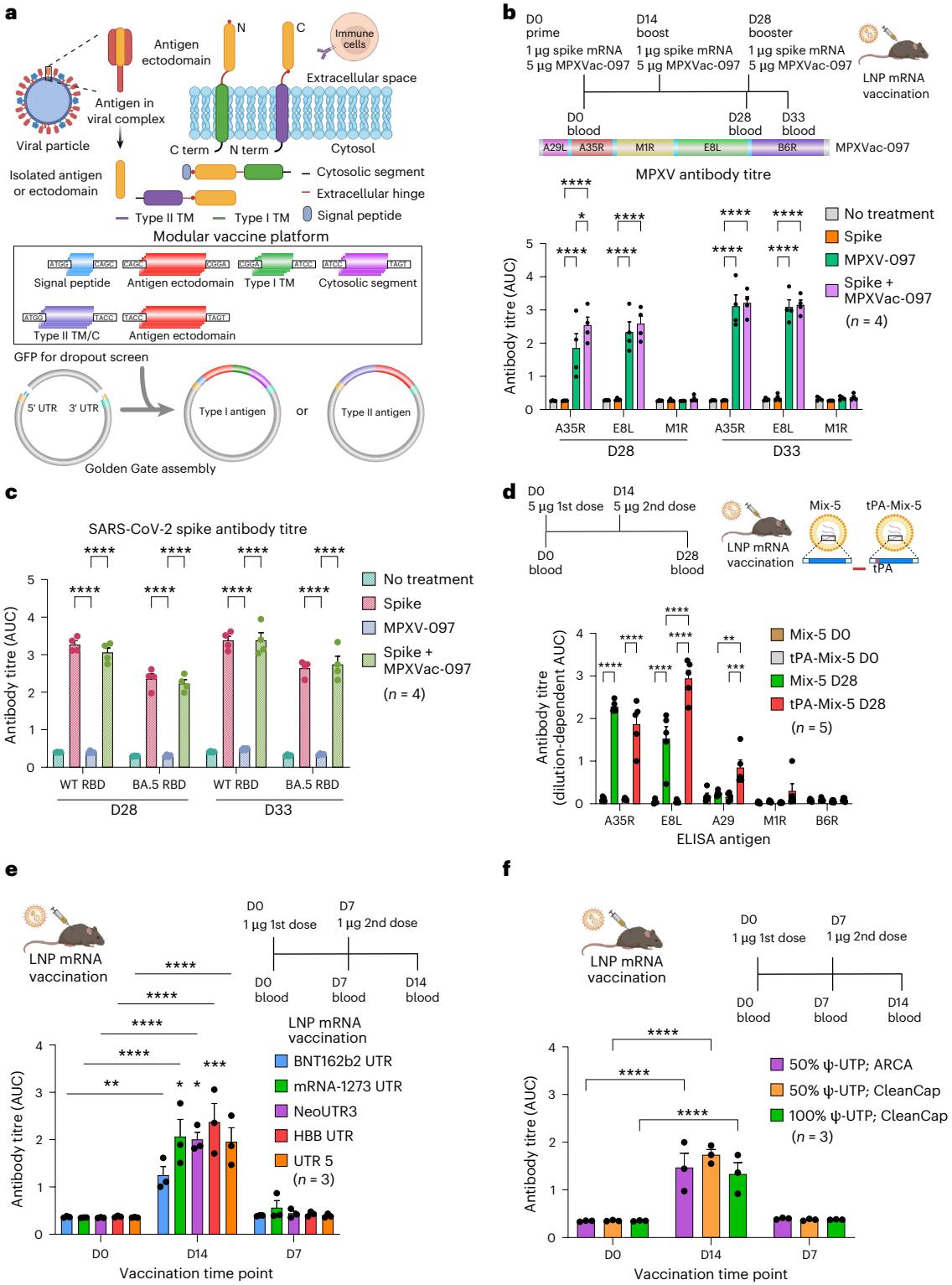

Fig. 1 | The MVP enhanced the immune response of MPXV mRNA antigens in mice. a, Schematic of the MVP displaying distinct antigen epitopes through TM/C modules. **b**,**c**, Antibody titre plateaus (AUC = ~3) were observed after 2 doses of spike wild type (WT; **b**) and 3 doses of MPXVac-097 LNP mRNAs (**c**), revealing space for mpox antigen optimization. No treatment group was excluded from the statistical comparisons. **d**, Effect of SP on antibody titre in mice. tPA SPs significantly enhanced antibody titres of type I E8L and cytosolic A29. Statistical comparisons were made between groups with matching dates or treatments. **e**, Effect of UTR on A35R antibody titre in mice. A35R LNP mRNA with different 5′ and 3′ UTR pairs elicited a significant antibody response in mice ($n = 3$). Antibody titres on day 14 were compared with those on day 0 or with BNT162b2 in the day 14 subgroup. Statistical comparisons were made between treatment groups on day 14. **f**, Effect of nucleotide composition (cap structure and pseudo-UTR abundance) on the immunogenicity of A35R mRNA antigens (that is, the A35R antibody titre) in mice. Statistical comparisons were made between day 0 and the other time points. In **b**–**f**, the data represent means ± s.e.m. Statistical significance (*$P < 0.05$; **$P < 0.01$; ***$P < 0.001$; ****$P < 0.0001$) was determined by pair-wise Tukey's comparison test (**b**–**e**) or Dunnett's comparison test (**f**). D, day; term, terminal; RBD, receptor binding domain; Mix-5, mixture of five single antigen LNP mRNAs; ψ-UTP, pseudouridine-5′-triphosphate. Panel **a** (top) and mouse icons in **b** and **d**–**f** created with BioRender.com.

and translation efficiency, whereas TM/C domains influence the subcellular localization and surface expression of antigens. To investigate the impact of these elements, we first tested five UTR sequences derived from UTR screen studies[25–27] and the BNT162b2 (ref. 22) and mRNA-1273 (ref. 23) vaccines. We fused the respective LNP mRNAs of A35R with different UTRs and vaccinated immunocompetent C57BL/6 (B6) mice using a two-dose intramuscular administration with a one-week interval between doses (Fig. 1e and Supplementary Table 3). On days 0, 7 and 14, we collected blood samples from the immunized mice and analysed antibody titres against A35. Although all five UTR groups elicited significant antibody titres, three UTRs (mRNA-1273, neoUTR3 and HBB UTR) produced stronger antibody responses in mice at day 14 post-immunization compared with the UTRs from the Food and Drug Administration-approved SARS-CoV-2 vaccine (BNT162b2) (Fig. 1e and Supplementary Fig. 5). These findings indicate that optimizing UTR sequences can enhance the immunogenicity of mRNA vaccines, leading to more robust antibody responses.

Cap structure and pseudo-UTP abundance have been shown to influence protein transcription and immune response[28,29]. In addition to UTR sequences, we analysed the effects of cap structure and pseudo-UTP abundance in combination with the BNT162b2 UTR on A35 antigen expression and immunogenicity. Antigen expression was evaluated in HEK293T cells (Supplementary Figs. 6–8), and immunogenicity was assessed after two-dose immunizations in vivo. Modifying the nucleotide composition using 50% pseudo-UTP and a CleanCap structure resulted in a trend of higher antibody titres and reduced variation between samples (Fig. 1f). Based on these observations, we selected this nucleotide composition for further experimentation.

To evaluate the relationship between antigen cellular expression levels and immunogenicity, we tested the expression of A35R in cells transfected with plasmid DNA or LNP mRNAs with different UTR, RNA cap and pseudo-UTP compositions. All A35R DNA plasmids and LNP mRNAs were strongly expressed in HEK293T cells, as indicated by the normalized PE integral (that is, the normalized AUC value from the fluorescence intensity histogram for the phycoerythrin-conjugated antibody; Supplementary Fig. 6) in flow surface staining (Supplementary Figs. 6–8). The UTR, RNA cap and pseudo-UTR play important roles in mRNA stability, transcription initiation and immune recognition. To investigate the effects of UTR and nucleotide modification on mRNA stability before immunization, we measured the decay curves of different LNP mRNAs by quantifying A35 antigen expression in HEK293T cells transfected with LNP mRNAs stored at 4 °C for 0, 9 and 16 days before use. The antigen level exhibited a linear decay over these time points, with decay rates shown as the slopes of linear regression (Supplementary Fig. 6c,d). Although no significant linear correlation was found between antigen expression levels and antibody titres (Supplementary Fig. 6e), UTRs used in commercial vaccines exhibited high antigen expression levels and were identified in unsupervised hierarchical clusters (circled), where antibody titres showed positive correlations with antigen surface expression.

The MVP enhances the immunogenicity of type II and cytosolic antigens

Due to the regional or partial correlation between an antigen's cellular expression and its in vivo immunogenicity, we sought to identify TM/C modules that can enhance antigen expression and immunogenicity. To evaluate type II TM/C module characteristics, we created a type II TM/C library containing TM/C domains of A35R, three endomembrane proteins and 34 human single-pass transmembrane proteins on the cell membrane. These TM/C modules were recombined with A35R ectodomain (A35Re) and expressed in 293T cells. To identify the best type II TM/C modifications that can enhance CST, we then performed a mini-screen of this library. Using flow cytometry, we quantified the antigen surface expression mediated by TM/C modules (Methods and Fig. 2a). The mini-screen indicated that FIBCD1, KEL and TNFSF13B TM/C modules mediated the highest A35Re surface expression in both antigen-positive (PE^+) and high-antigen-density (PE-high) populations. Negative controls and endomembrane chimeras exhibited minimal cell surface signals (Fig. 2a, Extended Data Fig. 1 and Supplementary Fig. 9a,b). To understand features associated with strong CST signals, we plotted antigen expression levels (PE rate × mean fluorescence intensity (MFI)) against several TM/C protein features, including RNA concentration in blood, RNA concentration in single-cell transcriptomes (Human Protein Atlas) and TM/C module sequence length (Fig. 2b and Supplementary Fig. 9c). Interestingly, TM/C-module-mediated antigen expression was negatively correlated with TM/C module length and showed no notable correlation with RNA concentrations. This suggests that compact modules generate stronger CST signals, whereas RNA concentration alone is not a reliable predictor of antigen expression levels mediated by the TM/C modules.

Next, we repeated the mini-screen with type I and II TM/C modules to identify the best modifications that can enhance the CST and immunogenicity of cytosolic antigens. We focused on mpox A29, a typical cytosolic model antigen whose native orientation on viral particles remains unclear. A29 was recombined with type I (with spike SP) or type II TM/C modules to display different antigen epitopes, allowing us to quantify and unify the CST strength of type I and II TM/C modules. To refine the type II TM/C testing set and ensure generalizability, only the top 21 TM/C modules from the A35R screen were further evaluated in the A29 CST screen. Using flow surface staining with anti-A29 antibody, the mini-screen demonstrated that the best-performing type II TM/C domains (fibrinogen C domain-containing protein 1 (FIBCD1), kell blood group antigen (KEL) and killer cell lectin-like receptor F1 (KLRF1)) exhibited increased CST compared with type I TM/C modules (chimeric antigen receptor (CAR), human leukocyte antigen (HLA) and the spike ESCRT- and ALIX-binding region (EABR)[30]) (Fig. 2c and Extended Data Fig. 2). Of note, KEL and FIBCD1 TM/C modules were identified as the top-scoring candidates, remarkably enhancing the surface expression of both A35R and A29, thereby supporting their generalizability in promoting antigen CST.

To characterize the effect of these TM/C modules on antigen immunogenicity, we packaged chimeric A29 selected from CST screens into LNP mRNAs. We then analysed the antibody and T cell responses of these LNP mRNA candidates in vivo and compared them with those of native A29 LNP mRNA. Remarkably, all six chimeric A29 variants elicited antibody titres two to three orders of magnitude higher than that of native A29 (Fig. 2d and Supplementary Fig. 10a). The T cell response, as indicated by cytokine secretion after A29 peptide stimulation, was significantly higher in chimeric A29 groups compared with native A29. Certain candidates enhanced specific subsets of cytokines: FIBCD1, spike and A35R TM/C domains for interferon-γ (IFNγ); A35R TM/C domains for interleukin 2 (IL-2); and KEL and A35R TM/C domains for IL-4 (Fig. 2e and Supplementary Fig. 10b,c). These findings indicate that chimeric A29 antigens with optimized TM/C modules significantly enhance both antibody and T cell responses, underscoring their potential for improving the immunogenicity of mRNA vaccines.

The MVP elevates the CST and immunogenicity of type I antigens

Building on the promising data from type II and cytosolic antigen optimization, we then optimized the type I antigen, M1R. To evaluate the CST strength of type I modules, we recombined type I SP and TM/C modules with M1R ectodomain (M1Re), quantified the surface expression of chimeras and normalized their expression levels with negative controls to minimize batch effects. We used the chimeric M1Re fused with HLA TM/C modules to assess the signal strength of different SP modules. Compared with the control M1Re–[HLA TM/C] (without SP), all SPs significantly enhanced M1Re surface expression. Among them, spike, secrecon, Env and CD8a SP led to the highest M1Re expression levels (Fig. 3a and Supplementary Fig. 11a). Based on this finding, we

https://doi.org/10.1038/s41551-025-01478-6

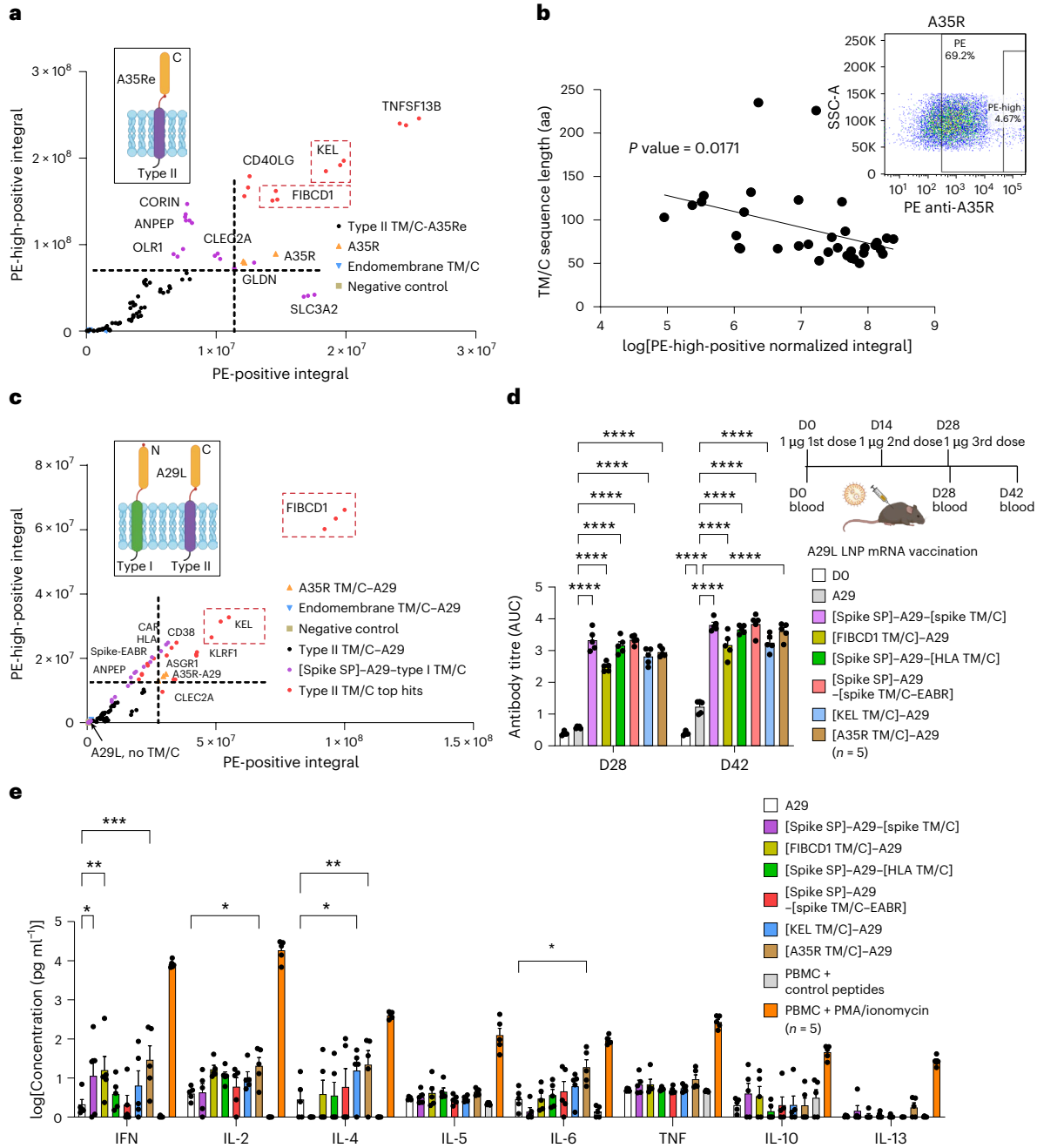

Fig. 2 | The MVP enhanced the CST and immunogenicity of type II and cytosolic antigens. a, Graph of the surface expression levels of A35Re fused to type II TM/C domains in 293T cells, quantified using flow surface staining, as normalized PE integrals in PE-positive (*x* axis) and PE-high-positive (*y* axis) populations ($n = 3$). **b**, Graph of the significant linear correlation between A35R chimera surface expression levels and TM/C domain sequence length. Simple linear regression test was used to determine significance. **c**, Effect of type I or II TM/Cs on A29 surface expression in 293T cells ($n = 3$). Dashed line highlights the potent modules found in **a** and **c**. **d**, Effect of TM/C on antibody response to A29. LNP mRNAs of chimeric A29 selected from **c** elicited significantly higher antibody responses than those of native A29 ($n = 5$). **e**, Effect of TM/C on A29 T cell response on day 42. Chimeric A29 LNP mRNAs elicited higher T cell responses than those of native A29 ($n = 5$). The data represent means ± s.e.m. In **d** and **e**, Dunnett's comparison test was used to determine the significance (*$P < 0.05$; **$P < 0.01$; ***$P < 0.001$; ****$P < 0.0001$) between A29 and the other treatment groups. aa, amino acids; K, thousand; SSC-A, side scatter area. Insets in **a** and **c** and mouse icon in **d** created with BioRender.com.

recombined Flag-tagged M1Re and untagged M1Re with the optimal SP (spike SP and CD8a SP, respectively). Then, we tested the surface expression of the chimeric TM/C modules using these two M1Re constructs (Fig. 3b and Supplementary Figs. 11b and 12). HLA, CAR and spike TM/C modules significantly increased M1Re antigen surface expression. The substantial antigen expression difference in [CD8a SP]–M1Re–[HLA TM + EPM–EABR] (where EPM–EABR represents an endocytosis prevention motif (EPM) fused to EABR)[30] and [spike SP]–M1Re–[E8L TM + EPM–EABR] highlights the importance of selecting appropriate combinations of CST signals for optimal antigen surface display.

To test whether these identified modules from the TM/C screens enhance immunogenicity in vivo, we performed immunizations with LNP mRNA candidates of M1Re antigen, engineered with TM/C modules identified in CST screens. We tested several different candidates,

https://doi.org/10.1038/s41551-025-01478-6

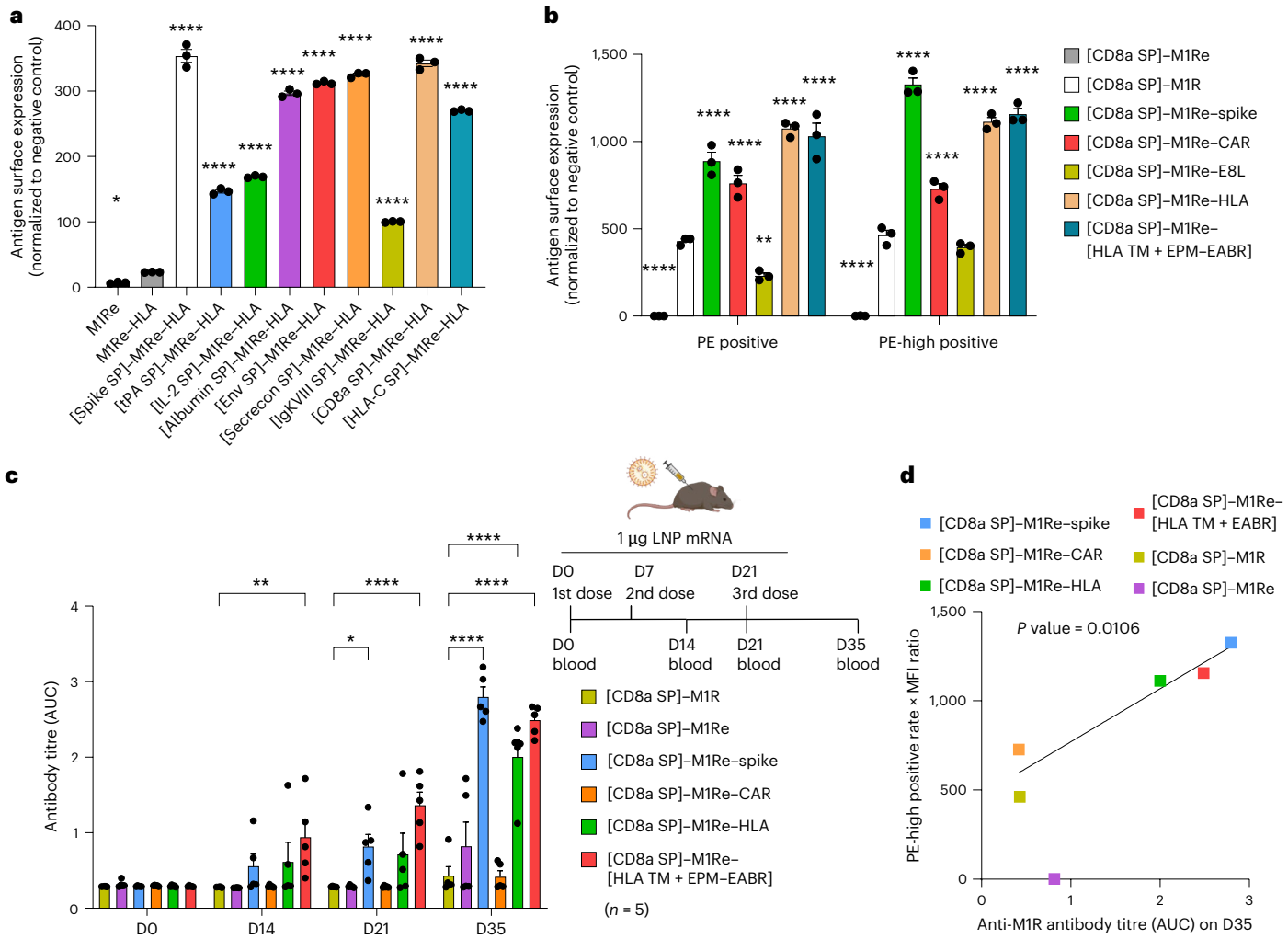

Fig. 3 | The MVP elevated type I M1Re surface expression and improved the immunogenicity of its LNP. a,**b**, SP (**a**) and TM/C (**b**) modules significantly enhanced the cell surface expression of chimeric M1Re (Flag-tagged M1Re–[HLA TM/C] in **a** and [CD8a SP]–M1Re in **b**; $n = 3$). **c**, Type I TM/C modules recombined with [CD8a SP]–M1Re significantly elevated the antibody response to chimeric M1Re LNP mRNA ($n = 5$). **d**, Antibody titres against recombined M1Re showed significant linear correlation with the corresponding antigen's CST in 293T cells. CST was quantified using the normalized PE-high integral and plotted against the anti-M1R antibody titre shown in **c**. All of the data points except for secreted M1Re were analysed using the linear regression model. Simple linear regression test was used to determine significance. The data represent means ± s.e.m. In **a**–**c**, Dunnett's comparison test was used to determine the statistical significance (*$P < 0.05$; **$P < 0.01$; ****$P < 0.0001$) between the controls and other treatment groups. The controls included M1Re-HLA (**a**) and [CD8a SP]–M1R (**b** and **c**). Mouse icon in **c** created with BioRender.com.

including HLA, CAR, EPM–EABR and spike, using a three-dose vaccination regimen in B6 mice. Blood samples were collected on days 0, 14, 21 and 35 after immunization (Fig. 3c and Extended Data Fig. 3a). We found that the M1R and M1Re groups without TM/C modification led to minimal antibody titres; in sharp contrast, the spike, HLA and HLA + EABR TM/C groups elicited potent antibody responses. Notably, the CAR-modified M1Re group did not show a heightened antibody response compared with the unmodified M1R control. Antibody titres were positively correlated with the antigen's surface expression, as quantified by the fluorescence integral of the PE-high population (Fig. 3d and Extended Data Fig. 3b). These data demonstrated that TM/C modifications such as spike, HLA and HLA + EABR can significantly increase the immunogenicity of challenging antigens such as M1R.

To investigate cellular responses, we then characterized the T cell response profiles from vaccinated mice. Plasma and peripheral blood mononuclear cell (PBMC) samples were collected on day 35 after immunization and their culture media were analysed by bead-based multiplex cytokine profiling assay for cytokine secretion. The M1Re group (ectodomain only) showed a relatively low T cell response (Fig. 4a). Compared with M1Re, the unmodified M1R group exhibited upregulated IL-4 and IL-5 production by T cells. M1Re with selected TM/C modifications showed enhanced cytokine production (for example, the CAR group for IFNγ, IL-5 and IL-4 production and the HLA group for IL-10 production). Among the measured cytokines, IFNγ, tumour necrosis factor α (TNFα) and IL-2 are the main type 1 T helper cell (T_H1 cell) cytokines associated with cell-mediated immunity and inflammation, whereas IL-4, IL-5 and IL-10 are classic T_H2 cytokines mediating antibody response and anti-inflammatory response[31,32]. Dot plots indicating IFNγ and IL-4 cytokine concentrations revealed balanced T_H1 and T_H2 responses in all vaccination groups induced by chimeric M1R (Fig. 4b). To evaluate the effects of TM/C modules on T_H1/T_H2 balance, we defined T_H1/T_H2 skewness as the distance to the symmetry line $y = x$ on a two-dimensional plane of T_H1 and T_H2 cytokines. The spike TM/C chimera elicited a stronger T_H1 response after M1R peptide stimulation, whereas HLA + EABR and M1R TM/C modules led to higher T_H2 responses (Fig. 4b, inset). Compared with the native A29 group, the T_H1/T_H2 plot showed a consistent increase of T_H1 and T_H2 responses mediated by CST modules. The skewness data indicated that spike

https://doi.org/10.1038/s41551-025-01478-6

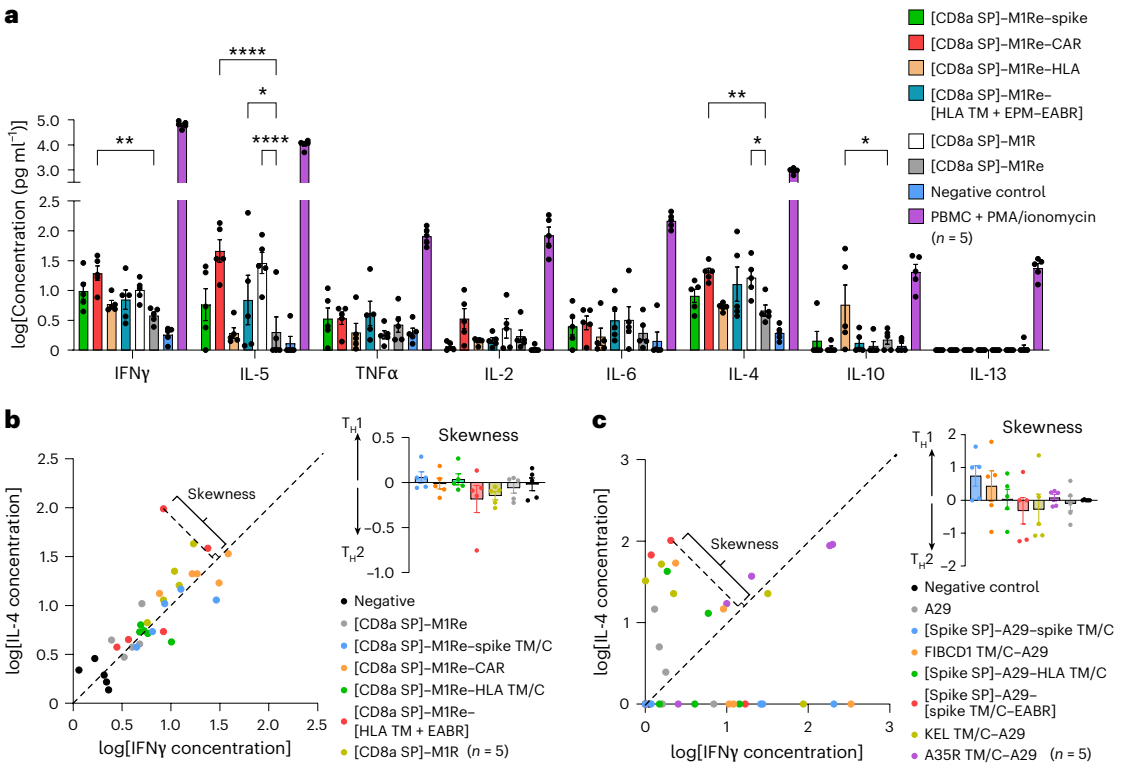

Fig. 4 | The MVP elevated type I M1Re surface expression and improved the immunogenicity of its LNP mRNAs. a, Chimeric [CD8 SP]–M1Re with different TM/C modules exhibited stronger T cell responses than secreted M1Re, as indicated by the cytokine secretion from M1R-peptide-stimulated T cells on day 35 ($n = 5$). The data represent means ± s.e.m. Dunnett's comparison test was used to determine the statistical significance (*$P < 0.05$; **$P < 0.01$; ****$P < 0.0001$) between [CD8a SP]–M1Re controls and the other treatment groups. **b**,**c**, Scatter plots showing the intensity and skewness of T_H1 and T_H2 responses to M1R (**b**) and A29 (**c**) peptide stimulation ($n = 5$). The log-transformed concentrations of IFNγ and IL-4 cytokines from **a** (M1R) and Fig. 2e (A29) were used to represent the T_H1 and T_H2 responses, respectively. The skewness was calculated from the dot distance to the symmetry axis $y - x = 0$ of the T_H1 and T_H2 responses on a two-dimensional plane.

and FIBCD1 TM/C modules mediated stronger T_H1 responses, whereas spike EABR and KEL TM/C modules were prone to inducing stronger T_H2 responses (Fig. 4c).

Next, we analysed the magnitude of both T cell and antibody responses for each TM/C chimera group. We found that the spike and HLA + EABR groups elicited potent antibody and T cell responses. In contrast, the CAR and M1R TM/C modules resulted in particularly high T cell responses (Extended Data Fig. 3c), although their antibody responses were much lower (Fig. 3c). These data demonstrated that the selected TM/C modifications not only enhance T cell and antibody responses, but also modulate T_H1 and T_H2 balance, highlighting their roles in regulating the immunogenicity of mRNA antigens.

Analysis of the CST strength of MVP modules and dependent factors

To systematically evaluate the CST strength of type I modules, we recombined type I SP or TM/C modules with multiple antigen ectodomains, quantified the surface expression levels of chimeras and normalized their expression levels with the maximum value in each antigen subgroup. These normalized antigen expression levels were designated as CST scores. We integrated CST scores from different MPXV antigen datasets and analysed these integrated scores, revealing variations in the CST signals of SP and TM/C modules across multiple antigen datasets (Fig. 5a,b, Extended Data Fig. 4 and Supplementary Figs. 13–15). The SP modules displaying high CST scores (CST > 0.7) and small variations between antigen datasets included spike, albumin and Env SP. Compared with SP modules, the integrated CST scores of TM/C modules exhibited larger variations between TM/C groups and antigen datasets. This analysis revealed that the HLA TM/C module is the most robust, producing the strongest antigen surface expression across different antigens (A29 and M1R), as measured by integrated CST score. Additionally, CAAX, spike, CAR and HLA + EABR modules also exhibited high integrated CST scores.

To analyse the signal strength of CST modules in different cell lines, we expressed chimeric A29–[HLA TM/C] with or without CD8a SP in 293T, B16F10, RAW264.7 and DC2.4 cells. Spike and GFP were used as controls to separate cell-line-dependent factors such as transfection efficiency, optimal antigen expression levels and background noise caused by PE staining (Fig. 5c and Supplementary Fig. 16). Interestingly, [CD8a SP]–A29–HLA showed significantly higher surface antigen expression levels than A29–HLA at all three time points for 293T cells, at late time points (24 and 48 h) for B16F10 cells and at an early time point (10 h) for RAW264.7 cells. The RAW264.7 and DC2.4 cell lines, derived from APCs, were notably less susceptible to lipofectamine transfection, as evidenced by their GFP levels, which were five- to 100-fold lower than those of 293T cells. Both RAW264.7 and DC2.4 cells showed a trend of A29–HLA increase (independent of CD8a SP) and a spike decrease over time. Intrigued by the distinct antigen expression behaviours of APC cell lines, we further investigated the impact of various SPs on A29–HLA expression in RAW264.7 and DC2.4 cells (Fig. 5d and Supplementary Figs. 17 and 18). Consistent with our observations in Fig. 5c, most SPs led to an expression level similar to that of A29–HLA except for secrecon SP, which showed much higher antigen expression in RAW264.7. Unexpectedly, the analysis of TM/C modules in RAW264.7 revealed that the increase in A29 antigen on the RAW264.7 cell surface was independent of TM/C membrane anchors (Fig. 5e and Supplementary Fig. 19). This suggests that antigen display on APC-related cells is associated with peptide degradation and presentation events. Together, these data

https://doi.org/10.1038/s41551-025-01478-6

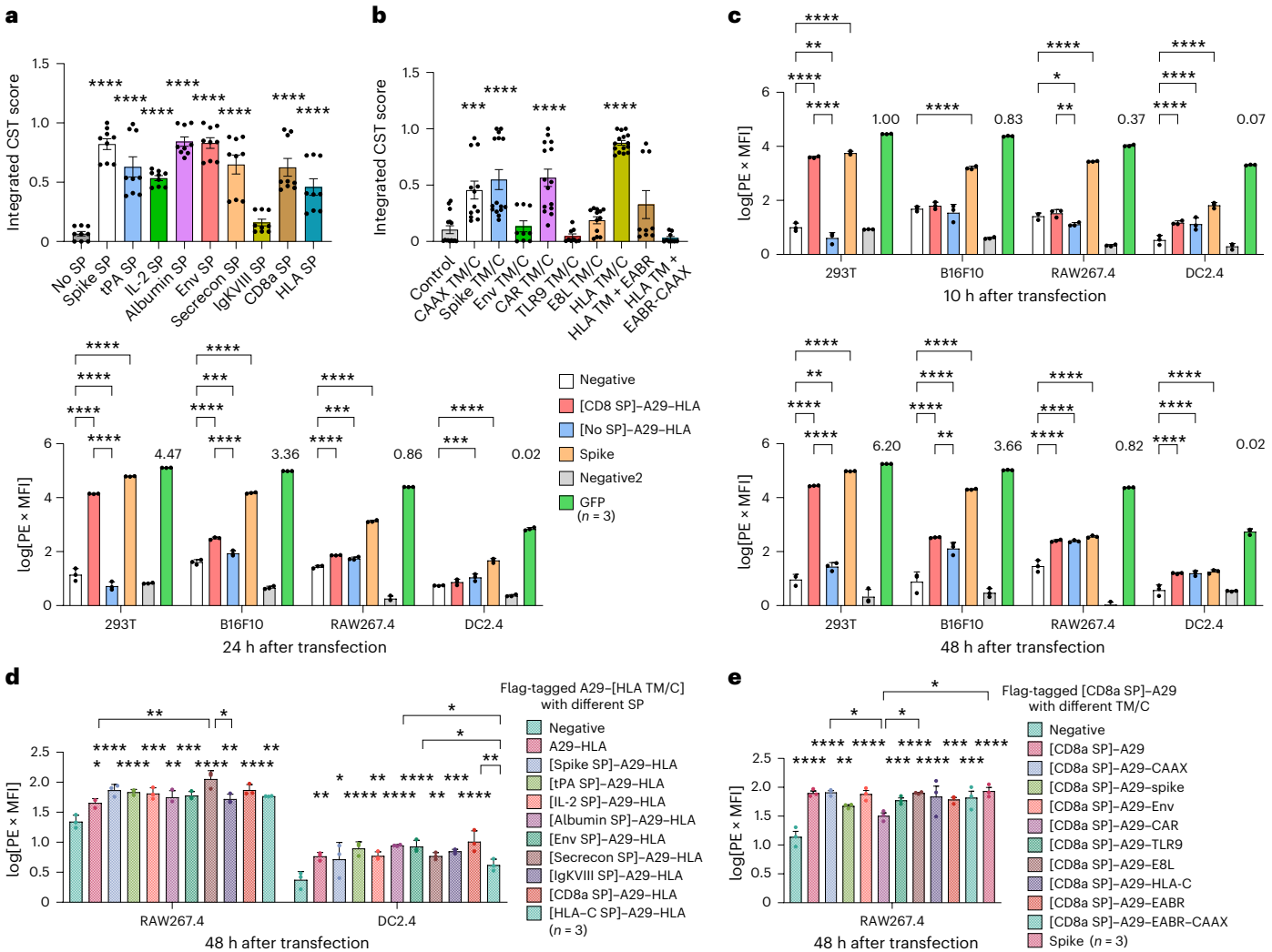

Fig. 5 | The surface translocation strengths of the MVP modules fluctuated as a function of antigen sequence, transfection time and expression cell line. a,**b**, Type I SP (**a**) and TM/C (**b**) modules led to a consistent increase in MPVX antigen expression on 293T cell surfaces, despite ectodomain-dependent variations. Integrated CST scores of SP (**a**; $n = 9$) and TM/C modules (**b**; $n = 15$, except for certain groups that were dropped out due to subpar performance; details in Source Data Figs. 1–8 and Extended Data Fig. 6) were evaluated as normalized antigen surface expression (shown in Extended Data Fig. 4). Statistical comparisons were made between controls and the other treatment groups. **c**, CD8a SP signal strength was influenced by time after transfection and expression cell type ($n = 3$). Only comparisons with the negative control or between two A29–HLA groups are shown. Negative2 represents a matched control for GPF group that did not undergo flow staining, whereas Negative underwent flow staining. **d**, Flag-tagged A29–[HLA TM/C] led to significant antigen expression on RAW264.7 and DC2.4 cell surfaces, regardless of SPs ($n = 3$). **e**, Anti-Flag flow surface staining showed that Flag-tagged [CD8a SP]–A29 surface presentation in RAW264.7 cells did not rely on TM/C membrane anchors ($n = 3$). The statistical comparisons without brackets (asterisks or values above plots) represent comparison with the negative control. The data represent means ± s.e.m. Statistical significance (*$P < 0.05$; **$P < 0.01$; ***$P < 0.001$; ****$P < 0.0001$) was determined by Dunnett's comparison test (**a** and **b**) or pairwise Tukey's comparison test (**c**–**e**).

indicate that CST module signal strength fluctuates depending on the antigen sequence, expression cell line and time point.

The MVP enhances MPXV LNP mRNA effectiveness in viral challenges

Next we investigated whether chimeric antigens with CST-enhancing modules would provide better protection against vaccinia virus (VACV) lethal challenge. On days 0 and 7, mice were intramuscularly vaccinated with 4 μg LNP mRNAs encoding A29, M1R or A29 + M1R, with or without CST-modifying modules, followed by an intranasal lethal challenge of VACV on day 21. MPXVac-097 was used as a positive protection control that fully protected immunized mice from death, weight loss and signs of infection. Unvaccinated mice and mice vaccinated with A29 LNP mRNA showed evident weight loss after challenge and succumbed to infection by day 6 after challenge (Fig. 6a–c). The percentages of mice vaccinated with unmodified M1R or A29 + M1R LNP mRNAs that survived until the study endpoint were 40% and 80%, respectively. Compared with native antigen vaccination groups, the chimeric antigen groups consistently exhibited faster weight recovery, milder disease signs and higher survival rates (Fig. 6a–c). These results suggest that chimeric mRNA antigens with enhanced CST provided better protection against lethal viral challenge.

The MVP is generalizable to the optimization of diverse mRNA antigens

To demonstrate the generalizability of the MVP, we went on to optimize additional type I transmembrane and nuclear antigens from VZV and HPV using a set of the most effective MVP modules. Type I VZV glycoprotein E (gE) and soluble HPV16 E6 and E7 are well-characterized vaccine targets and their LNP mRNAs have shown evident efficacy in

https://doi.org/10.1038/s41551-025-01478-6

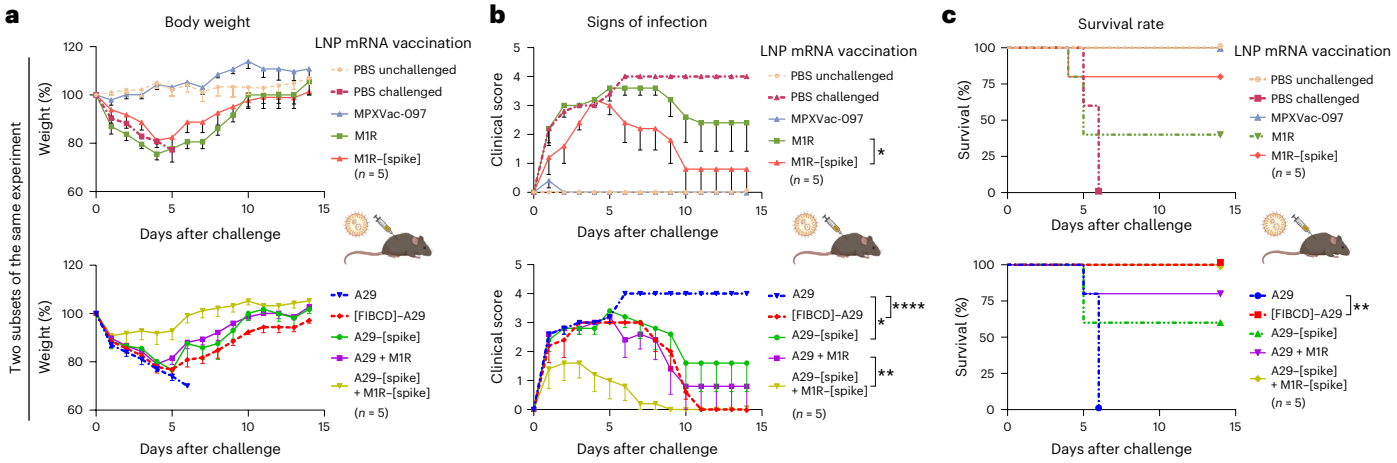

Fig. 6 | MVP-modified MPXV LNP mRNA showed better protection efficacy than native antigens in lethal VACV challenges. Mice were vaccinated with 4 μg LNP mRNA of each antigen on days 0 and 7, followed by intranasal lethal challenge with VACV (Western Reserve strain) on day 21 (also referred to as day 0 after challenge; $n = 5$). **a**–**c**, Mice vaccinated with MVP-modified mRNA antigens showed faster body weight recovery (**a**), milder disease signs (**b**) and a higher post-challenge survival rate (**c**). Mice with ≥30% weight loss were sacrificed. The data represent means ± s.e.m. Statistical significance (*$P < 0.05$; **$P < 0.01$; ****$P < 0.0001$) was determined by pair-wise Tukey's comparison test (**a** and **b**) or log-rank test (**c**). Only comparisons between the native antigen and modified antigen groups are shown. Mouse icons created with BioRender.com.

preclinical studies[4,7,17,33]. However, comprehensive comparisons of the effects of membrane-targeting modules on mRNA antigen expression and immunogenicity remain to be explored. Here we sought to investigate whether the effective CST modules identified using MPXV antigens could be applied to the optimization of mRNA antigens from other pathogens.

For VZV gE, we recombined its ectodomain with spike SP, as well as spike TM/C or HLA TM/C. Compared with full-length gE, HLA chimera not only showed much higher surface expression levels in 293T cells, but also led to a significant increase in antibody titres in LNP mRNA vaccination models (Fig. 7a,b). VZV gE 1–573 Y569A was reported in previous studies[7] and used as an additional control. In addition to the antibody response, the antigen-stimulated T cells from the HLA chimera group showed higher activation-induced markers (AIMs) and differential cytokine secretion patterns (Fig. 7c–e, Extended Data Fig. 5 and Supplementary Figs. 21–23). In the first 10 h of antigen stimulation, T cells of the full-length gE group produced more IL-2 than other vaccination groups. However, cytokine levels became more comparable between full-length gE and HLA chimera after 30 h of stimulation. Overall, several of the TM/C-modified chimeric VZV gE vaccines produced a stronger antibody response and non-inferior T cell response.

For HPV16 E6 and E7, we fused non-oncogenic variants with representative type I or II modules (Supplementary Table 5). As expected, MVP modules significantly enhanced the surface translocation of antigen E7 in 293T cells (Fig. 8a). Despite the background in ELISA (Supplementary Fig. 20), spike TM/C LNP mRNAs elicited significantly increased antibody titres compared with those of the unmodified version against HPV E6 and E7 in animal vaccination models (Fig. 8b). In addition, after E6 + E7 peptide stimulation, T cells from the spike and FIBCD1 chimera groups showed consistently elevated AIM, cytokine production and secretion compared with unmodified E6 + E7 control vaccination (Fig. 8c–e and Supplementary Figs. 24 and 25). LNP mRNAs of spike and FIBCD1 chimera significantly boosted T cell killing ability against E6 + E7 peptide-pulsed B16 target cells, regardless of whether they were transduced with HPV16 wild-type E6 and E7 (Fig. 8f, Extended Data Fig. 6 and Supplementary Fig. 26).

Discussion

We have systemically compiled and evaluated CST modules for the purpose of mRNA antigen optimization. This enables rapid antigen assembly and provides a one-stop platform with which to optimize type I and II transmembrane antigens and soluble antigens, including nuclear[34] (E6 and E7) and cytosolic antigens (A29). We established a quantitative metric—the CST score—with which to evaluate the surface translocation strength of different CST modules. Using this CST score, we evaluated the CST strength of type I and II modules using multiple antigens and identified recurring modules that greatly enhanced the CST of multiple antigens. Distinct from pooled next-generation sequencing screens, every chimeric antigen sequence in our CST screens was confirmed through Sanger sequencing to ensure high fidelity of antigen sequences and CST signals. Furthermore, we quantified and unified the CST strength of type I and II modules using the A29 cytosolic antigen.

In addition, we characterized the effects of tPA SP on the immunogenicity of five mpox antigen LNP mRNAs. We found that this enhanced the antibody responses of A29 and E8L but did not increase responses to other antigens. Common SPs are located at the N terminus of type I transmembrane or secretory proteins. They are cleavable type II transmembrane domains evolved to adapt to type I transmembrane protein topology. Naturally, one would expect them to be more effective on soluble proteins and type I transmembrane proteins without native SPs, such as A29 and E8L (Supplementary Discussion).

The MVP offers diverse type I and II CST libraries for the display of distinct epitopes of soluble antigens and the induction of desired antibodies targeting different antigen regions. The MVP increased antigen surface expression levels by 100- to 10,000-fold, antibody titres by >200-fold and T cell responses by 2- to 20-fold. These data of antigen surface expression, antibody response and T cell response revealed a positive correlation between chimeric antigen surface expression and antibody response, whereas no obvious correlation was found between T cell response and antigen surface expression level. Chimeric antigen expression in APC cell lines showed an evident degradation of GFP and spike over time, as well as a membrane-anchor-independent display of Flag peptides on the cell surface, suggesting that the presentation of a folded or degraded antigen is dependent on the expression cell line and associated with antibody and T cell responses.

Unlike traditional antigens directly delivered to extracellular space, mRNA antigens originate from the cytosol of recipient cells, including cells around injection sites and draining lymph nodes[35]. These antigens

https://doi.org/10.1038/s41551-025-01478-6

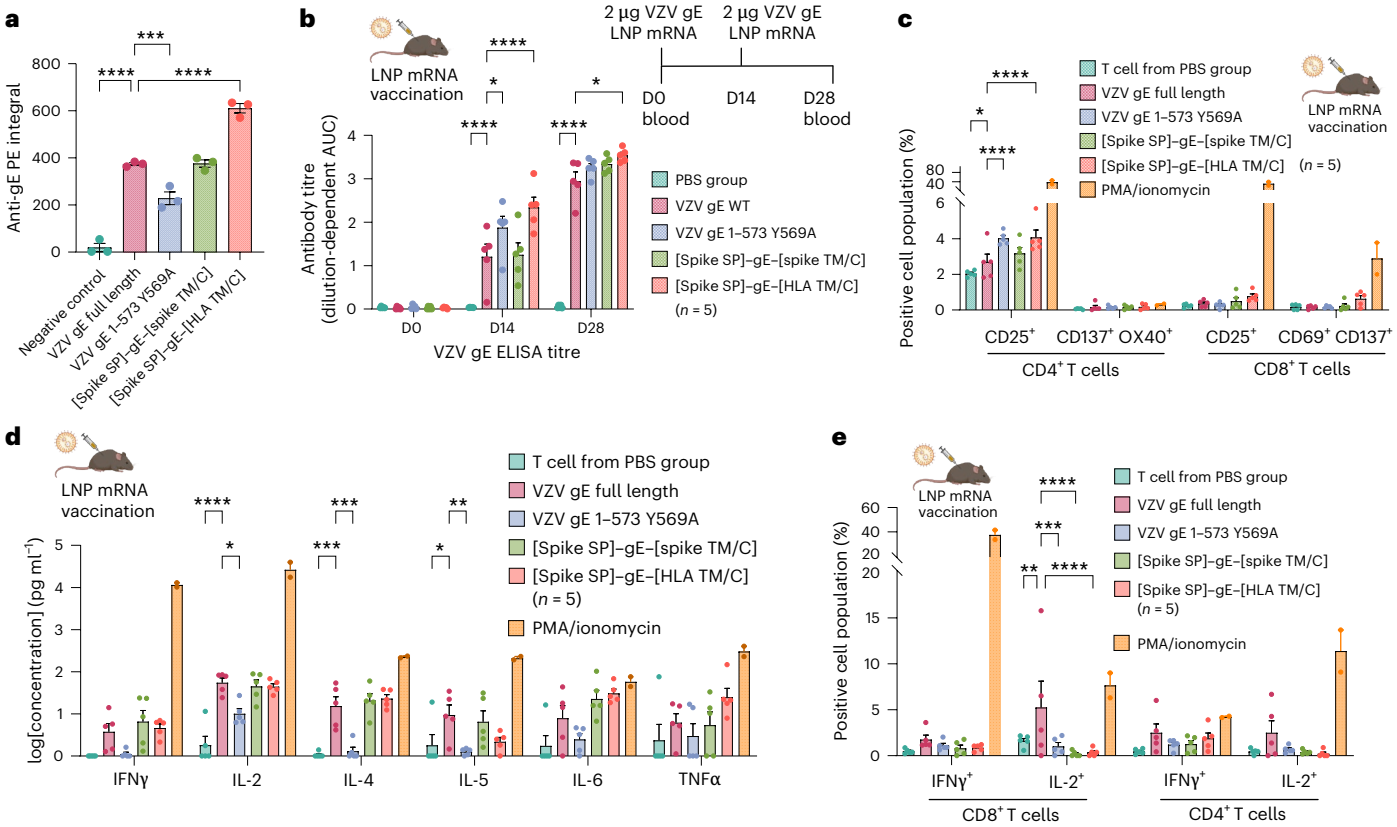

Fig. 7 | The MVP enhanced antibody and T cell responses to chimeric VZV gE LNP mRNA in animal models. a, MVP modules significantly increased VZV gE surface expression levels in 293T cells. VZV gE 1–573 Y569A was reported in previous studies and used as a control. **b**, MVP-modified gE LNP mRNAs mediated higher antibody responses than WT controls in the animal vaccination model. **c**, T cells collected on day 28 from mice vaccinated with modified gE LNP mRNAs showed higher AIM levels after gE antigen stimulation for 30 h. **d**,**e**, MVP-modified gE groups showed comparable cytokine secretion, or a trend of higher secretion, from T cells 30 h after antigen stimulation (**d**), whereas T cells of the VZV gE WT group displayed higher IL-2 production ~10 h after stimulation, as determined by intracellular cytokine staining assay (**e**). The data represent means ± s.e.m. In **a**–**e**, Dunnett's comparison test was used to determine the statistical significance (*$P < 0.05$; **$P < 0.01$; ***$P < 0.001$; ****$P < 0.0001$) between the VZV full-length gE (WT) group and the other treatment groups. The PMA/ionomycin group was excluded from the comparisons. The sample number for the vaccination groups was 5, except for PMA/ionomycin, of which sample number was 3. Mouse icons in **b**–**e** created with BioRender.com.

need to translocate to the extracellular space before they are recognized by immune cells. T cells recognize the antigen fragments degraded in APCs and presented by major histocompatibility complex (MHC) molecules, whereas B cells can recognize the intact antigens[36,37]. CST modules influence antigen presentation by regulating MHC class I and II pathways, which play key roles in T cell response and antibody response[37].

The data from soluble antigens, including M1Re, A29 and E6 + E7, suggested that enhancement of antigen CST via optimal modules often boosts both antibody and T cell responses (optimal modules in Source Data Figs. 1–8 and Extended Data Fig. 6). Our data from type I antigens, including M1R and gE, show that enhancing CST by replacing native TM/C modules boosts the antibody response and alters the T cell response in less predictable ways. For M1R, MVP modules (except for CAR TM/C) lowered the T cell response. For VZV gE, the HLA TM/C increased T cell activation and shifted cytokine secretion patterns compared with full-length gE. These data highlight an intricate relationship between membrane-targeting sequences, antibody response and T cell response. It is worth noting that the chimeric antigen LNP mRNA with enhanced CST universally led to better protection against lethal VACV challenge compared with native antigen LNP mRNAs, confirming the overall benefit of optimizing viral mRNA antigens and improving their CST.

Several case studies have shown that antigen presentation can be increased by coupling mRNA antigens to membrane-targeting sequences[17,38–40], highlighting the importance of enhancing the membrane trafficking of mRNA antigens for T cell and antibody responses. Compared with previous studies that used a single membrane-targeting sequence on a sporadic vaccine antigen, our study systematically screened, compared and unified CST strength of ~60 type I and II modules. Our unbiased screen and individual testing identified and validated multiple high-ranked effective modules that were previously un- or underused, including type I TM/C modules (HLA and spike TM/C modules), type I SPs (spike, Env and albumin SPs) and type II TM/C modules (FIBCD1 and KEL TM/C modules) (optimal modules in Source Data Figs. 1–8 and Extended Data Fig. 6). For example, FIBCD1 TM/C represents an optimal module of a new category of membrane-targeting sequences that has not been applied in mRNA vaccines before. This showed comparable or superior performance to the type I optimal module (spike TM/C) in the optimization of soluble antigens, including MPXV A29 and HPV E6 and E7. Using these modules as well as parental vectors with different UTRs, our current MVP version can generate ~2,500 and ~200 type I and II CST signal combinations, respectively, with any single antigen. Moreover, this system can be scaled up easily by harnessing the entire proteome of type I and II transmembrane proteins.

Importantly, we have demonstrated the robustness and universality of our MVP by applying the most effective MVP modules to the optimization of multiple antigens from different pathogens, including MPXV, VZV and HPV. The antigen and CST module libraries can be expanded easily to incorporate additional vaccine antigens and CST modules for the engineering of highly immunogenic LNP mRNA vaccines that mount potent B and T cell responses against specific antigens

https://doi.org/10.1038/s41551-025-01478-6

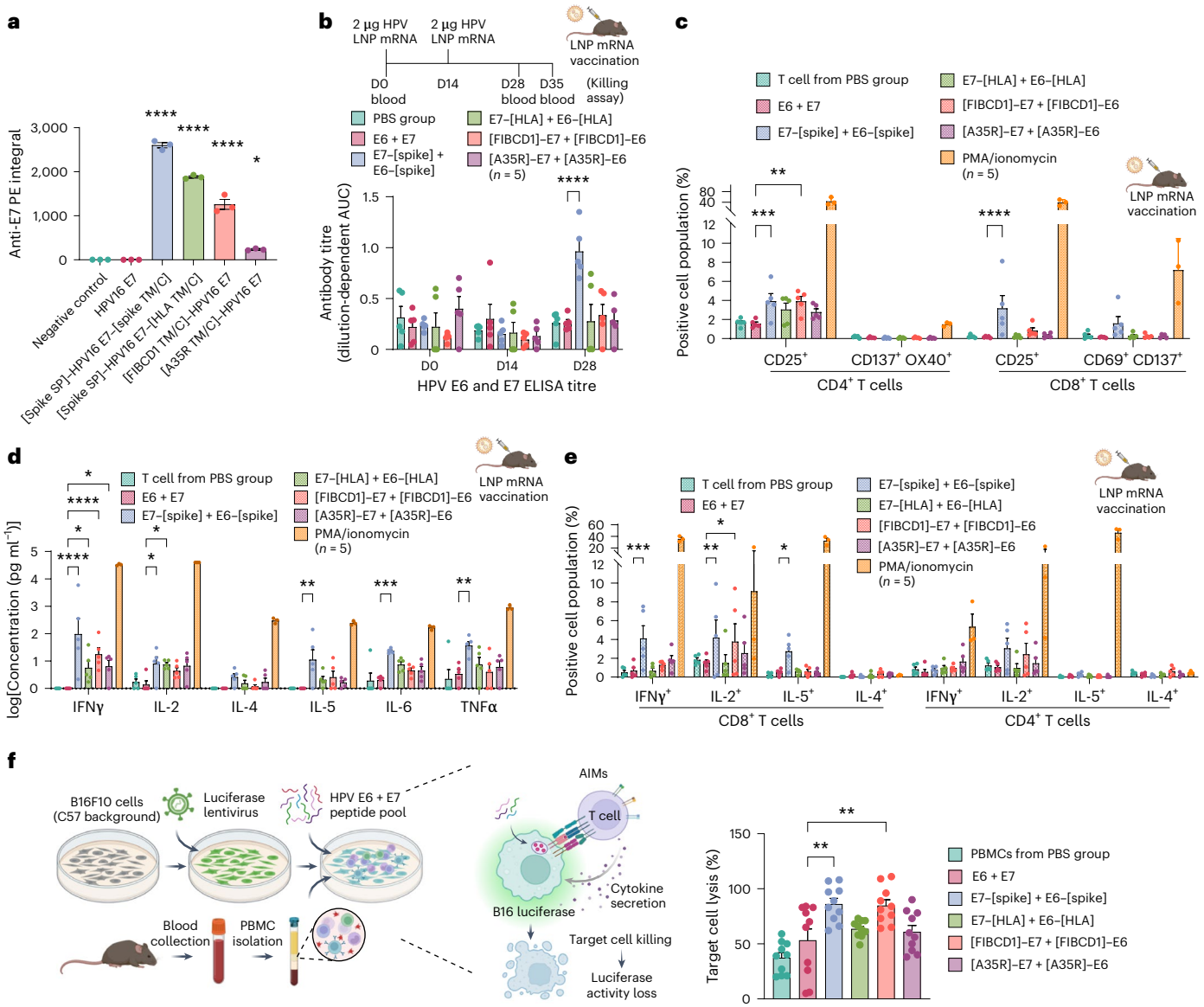

Fig. 8 | The MVP enhanced antibody and T cell responses to chimeric E6 and E7 LNP mRNA of HPV16 in mouse vaccination models. a, MVP type I and II modules boosted the expression levels of HPV16 E7 on 293T cell surfaces. **b**, LNP mRNA of E6 and E7 recombined with spike TM/C elicited significantly higher antibody titres than WT controls in mouse models. Blood samples were collected from mice vaccinated with 2 μg LNP mRNA to evaluate antibody and T cell responses ($n = 5$). **c**, Compared with the unmodified E6 + E7 vaccination group, higher AIM levels were observed in T cells collected on day 28 from mice vaccinated with MVP-modified mRNA antigens. Activation markers were surface stained in PBMCs, which were stimulated by E6 and E7 scanning peptide pools for 30 h. **d**,**e**, MVP-modified E6 + E7 LNP mRNA led to stronger cytokine secretion (**d**) and production (**e**) from T cells stimulated with E6 and E7 peptides for 30 h (**d**) or 10 h (**e**). For **e**, Brefeldin A was added to the media to block cytokine secretion in intracellular cytokine staining. **f**, Compared with control groups, T cells collected on day 35 from mice vaccinated with MVP-modified E6/E7 mRNA antigens led to higher cytolysis of B16F10 target cells pulsed with E6 and E7 peptides. To minimize variations from sample reading, two technical replicates of five biological samples were included in the target cell killing assay. The data represent means ± s.e.m. In **a**–**f**, Dunnett's comparison test was used to determine the statistical significance (*$P < 0.05$; **$P < 0.01$; ***$P < 0.001$; ****$P < 0.0001$) between the HPV16 E6 + E7 group and the other treatment groups. The PMA/ionomycin group was excluded from the comparisons. The number of biological samples in each vaccination group was 5, except for the PMA/ionomycin and target cell groups, of which sample number was 3. Panel **f** and mouse icons in **b**–**e** created with BioRender.com.

and/or pathogens. This versatile platform can be repurposed to display diverse proteins of interest on cell surfaces to induce antibodies targeting distinct epitopes. It also enhances our pandemic preparedness by facilitating mRNA vaccine development for other diseases. In addition, our MVP can potentially be applied to other areas, such as neoantigen mRNA vaccines, which have become a promising direction for personalized cancer therapy[41–43].

In summary, we established an MVP that provides a one-stop strategy for enhancing the CST of type I and II transmembrane antigens and soluble antigens. This platform can be used to enhance the immunogenicity of mRNA vaccines in terms of antigen cell surface expression, antibody titres, T cell responses and protection against infection, thereby providing a broadly applicable method for improving vaccine performance.

Methods

Institutional approval

Both recombinant DNA and biosafety work were conducted following the guidelines of the Yale Environmental Health and Safety Committee with approved protocols (Chen 18–45, 20–18 and 20–26). All of

the animal experiments were carried out following the guidelines of the Yale University Institutional Animal Care and Use Committee with approved protocols (Chen 2020-20358, Chen 2021-20068 and Lucas 2021-20375). This study did not involve human participants.

Plasmid cloning

The MPXV antigen sequences were cloned from the genome of a confirmed mpox case in the USA in 2022, as previously described[6]. VZV gE (strain Oka vaccine; UniProt ID Q9J3M8) and VZV gE 1–573 Y569A[7,44], HPV16 non-oncogenic E6 (UniProt ID P03126; C63G and Δ111–115, which corresponds to the deleted sequence CPEEK[4]) and HPV16 non-oncogenic E7 variant (UniProt ID P03129; C24G and E26G[4]) sequences are provided in Supplementary Table 5. The CST amino acid sequences were extracted from corresponding studies or UniProt as indicated in Supplementary Tables 1 and 2. They were codon optimized and synthesized at Integrated DNA Technologies, then inserted to the parental vector with 5′ and 3′ UTRs. Five UTR pairs were chosen based on the optimal sequences in clinical COVID-19 mRNA vaccines[22,23] or UTR screen studies[25–27] (Supplementary Table 1). Based on the in vivo immunization results of A35R LNP mRNA, HBB UTR pairs were used for all following plasmid cloning unless mentioned otherwise. The parental vector contained BsmBI-v2 digestion sites and GFP to enable rapid golden gate assembly (E1602L; New England Biolabs (NEB)) and dropout selection, respectively. GFP expression in *Escherichia coli* is driven by a prokaryotic promoter (BBa_J23100). Every chimeric antigen sequence in the CST screens was confirmed by Sanger sequencing.

CST sequence selection

The CST sequences were cloned from artificial constructs or single-pass transmembrane proteins localized on the plasma membrane in the human or viral proteome. The artificial constructs included secrecon SP[45], EPM–EABR[30] and CAR[46]. The type I and II CST sequences are listed in Supplementary Tables 1 and 2, respectively. To identify CST sequences, transmembrane proteins with a plasma membrane localization record in the Human Proteome Atlas were analysed. Their domain boundary, secondary structure, hydrophobicity, isoelectric point, protein sequence, size, membrane topology and cellular localization information was extracted (Supplementary Tables 1 and 2). Single-pass transmembrane proteins were the primary focus of this analysis because of their simple topology and compact signal sequences. Based on domain boundary and secondary structures, each transmembrane protein was divided into the following modules: SP (if any), ectodomain, extracellular hinge, transmembrane domain and cytosolic segment. Because of the drastic difference in surface charge between the plasma membrane and endomembrane, plasma membrane contacting sequences (extracellular hinge, transmembrane domain and cytosolic segment) would accommodate this unique charge property and contribute to the plasma membrane's specific localization. Therefore, the extracellular hinge, transmembrane domain, cytosolic segment and SP were identified as CST sequences and extracted from analysed transmembrane proteins. The CST modules are defined by their cleave sites (for SP), domain boundaries, secondary structures and hydrophobicity.

The type I CST library comprises nine SP, six TM domain and nine C segment constructs, which can give rise to approximately 500 combinations of type I CST signals. The type II CST library comprises the TM/C of A35R as an internal reference, three nuclear membrane or endomembrane proteins as negative controls (TMX4, SEC11A and POM121) and 34 type II single-pass transmembrane proteins on plasma membrane in the human proteome. The CST modules are defined by domain boundaries, secondary structures and hydrophobicity. The type I modules were selected based on the protein's popularity in the literature or industrial application. The type II modules were selected from the human proteome based on membrane topology and protein length. In total, 306 type I and 41 type II single-pass transmembrane proteins with plasma membrane localization recorded in UniProt or the Human Protein Atlas were identified in the human proteome. Out of 41 type II candidates, 34 were successfully cloned with compact module lengths, whereas the type I modules were selected based on the prevalence of the sequences in the literature and/or industrial application.

In vitro transcription of mRNA

The mRNA was in vitro transcribed from a linearized DNA template with different 5′ and 3′ UTR pairs using the HiScribe T7 ARCA mRNA kit (E2060; NEB) or the HiScribe T7 mRNA Kit with CleanCap Reagent AG (E2080; NEB). Either 50 or 100% N^1-methyl-pseudouridine (N-1081-5; TriLink) was incorporated during transcription. The transcribed mRNA was purified using a Monarch RNA Cleanup kit (T2040L; NEB) and kept at −20 °C.

LNP preparation

The mRNA was mixed with lipid mixture using a NanoAssemblr Ignite instrument as previously described[6]. The formulated LNP mRNA was diluted with phosphate-buffered saline (PBS) and buffer exchanged using a 100-kDa Amicon filter (89131-992; Macrosep Centrifugal Devices 100K). The mRNA encapsulation rate and mRNA concentration were determined by Quant-iT RiboGreen RNA Assay (R11490; Thermo Fisher Scientific). 8% sucrose (J21938; Affymetrix) was added to the final LNP mRNA sample before storing it at −80 °C in a freezer.

Cell culture

HEK293T (CRL-3216; ATCC), B16F10 (CRL-6475; ATCC) and RAW264.7 (TIB-71; ATCC) cells were maintained in Dulbecco's modified Eagle's medium (Thermo Fisher Scientific) with 10% heat-inactivated foetal bovine serum (FBS; HyClone), whereas DC2.4 cells were maintained in RPMI 1640 medium (Thermo Fisher Scientific) with 10% FBS. The DC2.4 cell line was a generous gift from L. Chen's laboratory at Yale University. Cells were passaged every two or three days at a split ratio of 1:3 or when confluency reaches over 95%. All of the cell lines tested negative for contamination with *Mycoplasma*.

Cell transfection with DNA plasmids or LNP mRNAs of MPXV antigens

293T cells were seeded to 24- or 48-well plates one day before transfection and were transfected with 1.0 or 0.5 μg plasmid DNA using a Lipofectamine 3000 transfection system (L3000015; Thermo Fisher Scientific). Two days after transfection, the cells were trypsinized and harvested for flow cytometry surface staining. Transfection was performed according to the manufacturer's protocol. For LNP mRNA transfection, 0.5 or 1.0 μg LNP mRNA was directly added to the cells one day after seeding and cells were collected after 20–24 h. Unless mentioned otherwise, most of the cell assay used DNA plasmid and Lipofectamine 3000 for transfection. In Fig. 5c, GFP was used to quantify the transfection efficiency of different cell lines. The GFP expression level in 293T cells at 10 h after transfection was normalized to 1. The SARS-CoV-2 spike served as a positive control antigen with known high enrichment on the cell surface.

Surface staining and quantification of MPXV antigens

After trypsinization, 293T cells overexpressing Flag-tagged MPXV antigens recombined with either SP or TM/C modules were washed once with MACS buffer (0.5% BSA and 2 Mm EDTA in PBS pH 7.4) and surface stained with PE anti-Flag antibody (637310; BioLegend; 1:100 dilution) on ice for 20 min.

The 293T cells overexpressing untagged MPXV antigens (A35R, M1R or A29) recombined with SP or TM/C modules were surface stained with anti-A35R (40886-M0026-100; Sino Biological), anti-M1R (IMSA-VACVL1R7D11C100UG (Innovative Research) or RVV13901B (Cell Sciences)) or anti-A29 (40891-M0032-100; Sino Biological) antibody (1:100 dilution; on ice for 20 min), washed once with MACS buffer and stained with PE anti-mouse secondary antibody (P-852; Fisher; 1:100

dilution on ice for 20 min). For the HPV and VZV antigen expression experiments, anti-VZV gE antibody (40907-MM12; Sino Biological), anti-HPV16/18 E6 with FITC fluorophore (sc-460 FITC; Santa Cruz Biotechnology) and anti-HPV16 E7 with PE fluorophore (sc-6981 PE; Santa Cruz Biotechnology) were used to detect antigen expression levels. After final staining, the cells were washed once with MACS buffer, and PE or PE-high positive cells were identified by flow cytometer (Attune NxT Software version 3.1 or BD FACSAria III Cell Sorter). FlowJo version 10.9.0 was used for flow cytometry data analysis. The antigen expression level on the cell surface was quantified by the PE-positive rate, the MFI in the PE-positive population and the PE-positive integral or normalized PE-positive integral. The PE-positive integral is the positive population MFI multiplied by the positive cell count. The normalized PE-positive integral is the positive integral over the gated cell count, which is the average integral per gated cell. It is equal to the positive MFI multiplied by the positive cell count divided by the total gated cell count, which is equivalent to the positive MFI multiplied by the PE-positive rate (normalized PE integral).

For the antigen surface expression mediated by TM/C modules, two PE thresholds were used to define PE and PE-high cell populations, because of potential changes in surface antigen density caused by TM/C modules. Different from UTRs or SPs, TM/C modules persist in antigen sequences and may influence antigen clustering and organization on the cell surface.

The antigen surface expression levels were further normalized by the maximum values within the subgroups. This normalization step enables comparisons between antigen datasets, represents the signal strength of the modules and is denoted as the CST score. The integrated CST score is calculated by averaging CST scores from multiple datasets and reflects the generalizable signal strength of modules and variations between antigens. For example, the CST scores or normalized antigen surface expression levels were derived from the normalization of datasets. The integrated CST scores in Fig. 5a,b were merged with the CST scores of Extended Data Fig. 4e,f to estimate the average CST strength of the modules and variations across different antigen sets.

Integrated CST score calculation

The universal CST score represents the strength of a signal sequence to translocate antigens or proteins to the cell surface. It is calculated from the average normalized surface expression of multiple antigens. Two consecutive normalization processes were performed on the PE-high positive rate × positive MFI ratio relative to the background, which was first normalized with the no-signal (no-SP or no-TM/C) control to obtain the expression fold change due to the SP or TM/C signal sequence and then further normalized with the maximum value in the signal sequence group. Calculation details can be found in Source Data Figs. 1–8 and Extended Data Fig. 6.

Mouse immunization

Female C57BL/6Ncr mice aged 8–10 weeks from Charles River Laboratories were immunized with two or three doses of LNP mRNA of different antigens on days 0, 14 and 28 or days 0, 7 and 21. The mice were maintained at 40–60% humidity under ambient room temperature and a 14 h day/10 h night cycle. Retro-orbital blood was drawn using Drummond capillary tubes (503020; Thermo Fisher Scientific) and collected in Eppendorf tubes with 10 µl 50 mM EDTA (pH 8) at the indicated time points. In Fig. 1b,c, the third immunization of spike on day 28 used 0.5 µg wild-type + 0.5 µg BA.5 spike LNP mRNAs.

Isolation of PBMCs from blood

The collected blood samples were diluted with an equal volume of 2% FBS and added to Lymphoprep Density Gradient Medium in SepMate-15 tubes (STEMCELL Technologies). The red blood cells, PBMCs and plasma were isolated from blood by centrifugation at 1,200*g* for 20 min. After centrifugation, approximately 200 µl diluted plasma was collected from the surface layer and the PBMCs in the remaining solution in the top layer were poured into a new tube. The separated PBMCs were washed with 2% FBS and the remaining red blood cells were lysed with ACK lysis buffer (A1049201; Gibco). ACK lysis of PBMCs was stopped with 2% FBS in PBS and the cell number was counted using an automated Corning cell counter (6749; Corning).

Functional T cell response assay

Approximately 0.3–0.5 million PBMCs from each mouse were cultured in a 96-well U-bottom plate in 200 µl complete RPMI medium with 10% FBS, 50 µM 2-mercaptoethanol, 1 µg ml^{-1} LEAF Purified anti-mouse CD28 Antibody (102116; BioLegend), Non-Essential Amino Acids (11140050; Gibco), GlutaMAX (35050061; Gibco), 1 mM sodium pyruvate (11360070; Gibco) and penicillin–streptomycin (15140122; Gibco). The positive control samples were stimulated with eBioscience Cell Stimulation Cocktail (500×; 00-4970-93; Thermo Fisher Scientific; PMA and ionomycin). Custom scanning peptide pools of mpox M1R and A29 (GenScript), commercial scanning peptide pools of HPV16 E6 (130-095-997) and E7 (130-095-999) (both Miltenyi Biotec) or VZV gE recombinant protein (GLE-V52H3-100ug; ACROBiosystems) were added at a final concentration of 2 µg ml^{-1} to PBMCs from vaccinated or unvaccinated mice (PBS control). PBMCs were cultured overnight in the presence of stimulating peptides or protein antigens. The supernatant was collected at the indicated time points and secreted cytokines in media were quantified using a mouse T_H1/T_H2 8-plex LEGENDplex kit (741054; BioLegend) following the manufacturer's instructions. The stimulated PBMCs were used for AIM assays.

AIM assay

The AIM assays were performed following established protocols described previously[47,48]. Quantification of activated T cells was determined by assessing the proportion of AIM$^+$ T cells including CD4$^+$ T cells that were also CD25$^+$ or OX40$^+$ CD137$^+$ and CD8$^+$ T cells that were also CD25$^+$ or CD69$^+$ CD137$^+$ after a 30-h antigen stimulation. Briefly, PBMCs were isolated, cultured and stimulated according to the protocols described in the sections above. For surface staining, 0.3–0.5 × 10^6 PBMCs were resuspended in PBS, stained with LIVE/DEAD Aqua Dead Cell Stain (Thermo Fisher Scientific; 1,000× in PBS) on ice for 20 min and then rinsed with PBS. Subsequently, the remaining surface antibodies in MACS buffer were added to the cells and incubated for 30 min at 4 °C in the dark. After surface staining, the cells were washed once with MACS buffer containing 2 mM EDTA and 0.5% BSA. The cells were immediately acquired using a BD FACSAria II Cell Sorter (BD Biosciences). The antibodies employed in this panel were CD3 PE/Cy7 (clone 17A2; BioLegend; 1:100), CD8a BV421 (clone QA17A07; BioLegend; 1:100), CD4 FITC (clone GK1.5; BioLegend; 1:100), CD25 BV650 (clone PC61; BioLegend, 1:100), CD69 APC/Cy7 (clone H1.2F3; BioLegend; 1:100), CD137 PE (clone 17B5; BioLegend; 1:50) and CD134 PerCP/Cy5.5 (OX40, clone OX-86; BioLegend; 1:50).

Intracellular cytokine staining

Brefeldin A (BioLegend) was added to PBMC culture media simultaneously with the HPV scanning peptide pools or VZV gE antigens (GLE-V52H3-100ug; ACROBiosystems). After 8–10 h of antigen stimulation, cells were stained with LIVE/DEAD Fixable Near-IR Dead Cell Stain (Invitrogen; 1:1,000 in PBS) for 20 min on ice. Samples were washed with MACS buffer (D-PBS with 2 mM EDTA and 0.5% BSA) and stained with surface stain cocktail containing the following antibodies[49]: CD3 PE/Cy7 (clone 17A2; BioLegend, 1:100), CD8a BV421 (clone QA17A07; BioLegend; 1:100) and CD4 FITC (clone GK1.5; BioLegend; 1:100) in MACS buffer on ice for 30 min. After surface staining, cells were washed with MACS buffer then fixed and permeabilized using the BD Cytofix/Cytoperm solution kit (554714; BD Biosciences) according to the manufacturer's instructions. Permeabilized cells were washed once and stained with intracellular cytokine stain cocktail containing

the following antibodies: IFNγ PE (clone W18272D; BioLegend; 1:100), TNFα Percp-Cy5.5 (clone MP6-XT22; BioLegend; 1:100), IL-2 BV510 (clone JES6-5H4; BioLegend; 1:100), IL-4 BV605 (clone 11B11; BioLegend; 1:100) and IL-5 APC (clone TRFK5; BioLegend; 1:100) for 30 min at 4 °C. Finally, cells were washed with MACS buffer and resuspended in 200 µl MACS buffer before running on a BD FACSAria II Cell Sorter (BD Biosciences). Analysis was performed using FlowJo software.

Lentivirus production

One day before transfection, HEK293T cells were seeded in 15-cm dishes to achieve 60–80% confluence at the time of transfection. One hour before transfection, culture media (Dulbecco's modified Eagle's medium with 10% FBS; D10) was replaced with 12 ml pre-warmed Opti-MEM medium (Invitrogen). For each dish, 450 µl Opti-MEM was mixed with 20 mg pXD023 plasmid (puromycin–luciferase plasmid; 192203; Addgene)[50], 15 mg psPAX2 (12260; Addgene), 10 mg pMD2.G (12259; Addgene) and 130 µl polyethylenimine (1 mg ml^{-1}). After a brief vortex, the mixture was incubated at room temperature for 15 min and then added dropwise to cells. At 3 h after transfection, Opti-MEM media was replaced with 20 ml pre-warmed D10 media. Viral supernatant was collected at 72 h after transfection, filtered using 0.45-mm filters (Fisher/VWR) to remove cell debris and then concentrated from 20 to 5 ml using Amicon Ultra 30 kD ultracentrifugation units (Millipore). The virus was then aliquoted and stored at −80 °C.

Target cell killing assay

B16F10 untransduced cells or cells transduced with wild-type HPV16 E6 and E7 were seeded in six-well plates and transduced with 1 ml concentrated puromycin–luciferase lentivirus at a virus-to-media volume ratio of 1:1. Two days after transduction, stable B16 cell lines were established by puromycin selection at 10 µg ml^{-1} concentration and maintained in 2 µg ml^{-1} puromycin media. One day before PBMCs were isolated from the blood of vaccinated mice, puromycin–luciferase target cells were seeded in white opaque 96-well plates (2 × 104 cells per well). The next day, target cells were incubated with 0.2–1.0 µg ml^{-1} HPV16 E6 plus E7 scanning peptide pools for 2–6 h. Then, the D10 media of target cells was removed and approximately 3–5 × 10^5 PBMCs (20–40% CD3$^+$ T cells) freshly isolated on day 35 were added to the target cells. The target cells and PBMCs were cultured in complete RPMI media supplemented with 2 ng ml^{-1} mouse IL-2 (212-12-20UG; PeproTech), 2 ng ml^{-1} mouse IL-12p70 (210-12-10UG; PeproTech), 10% FBS, 50 µM 2-mercaptoethanol, 1 µg ml^{-1} LEAF Purified anti-mouse CD28 antibody (102116; BioLegend), Non-Essential Amino Acids (11140050; Gibco), GlutaMAX (35050061; Gibco), 1 mM sodium pyruvate (11360070; Gibco) and penicillin–streptomycin (15140122; Gibco). At ~18 h after co-culture, PBMCs were gently resuspended in RPMI media and transferred to V-bottom plates. The culture media and PBMCs were separated by centrifugation and used for secreted cytokine assay and AIM assay, respectively. The target cell cytolysis was measured by adding 200 µl PBS with 150 µg ml^{-1} D-luciferin (PerkinElmer) to each well. The luciferase intensity was measured using a Plate Reader (PerkinElmer). Target cells without PBMCs were used as 0% cytolysis controls, whereas target cells incubated with PMA/ionomycin-treated PBMCs were used as 100% cytolysis controls.

ELISA

The commercial MPXV antigens used in the ELISA included A35R (40886-V08H; Sino Biological), M1R (40904-V07H; Sino Biological), A29 (A2L-M52H3 (ACROBiosystems) and 40891-V08E (Sino Biological)), E8L (E8L-M52H3; ACROBiosystems) and B6R (40902-V08H; Sino Biological). The A29 antigen from Sino Biological (40891-V08E) was found associated with higher background in ELISA and was replaced with A29 antigen from ACROBiosystems. Commercial VZV and HPV antigens used in the ELISA included VZV gE (GLE-V52H3-100ug; ACROBiosystems), HPV E6 (40963-V07E; Sino Biological) and HPV E7 (40965-V07E; Sino Biological). Antigens in PBS were coated at 3 µg ml^{-1} on a 384-well microplate (07-000-877; Fisher Scientific) in a cold room overnight. For HPV ELISA, 3 µg ml^{-1} E6 and 3 µg ml^{-1} E7 were simultaneously coated on the microplates. The next day, the plate was washed three times with PBST (0.05% Tween-20 diluted from 10× PBST stock; IBB-171; Boston BioProducts) on a 50 TS microplate washer (NC0611021; Fisher Scientific) and was blocked with 0.5% BSA (BP1600-100; Fisher Scientific) in PBST at room temperature for 1 h. Plasma was fourfold serially diluted with PBS at a starting dilution of 1:500. Then, 30 µl plasma diluent was added to the plate and incubated at room temperature for 1 h. After washing with PBST five times, the plate was incubated with anti-mouse IgG (H + L) secondary antibody (A16072; Thermo Fisher Scientific) for 1 h at room temperature. The secondary antibody with horse radish peroxidase was 1:2,500 diluted in 0.5% BSA blocking buffer before adding to the microplate. The plate was washed five times with PBST and developed with tetramethylbenzidine substrate (421101; BioLegend). After shaking for 20 min at room temperature, the reaction was stopped with 1 M phosphoric acid and the optical density at a wavelength of 450 nm (OD_{450}) was measured by multimode microplate reader (PerkinElmer EnVision 2105; Envision Manager version 1.13.3009.1401). A relatively high background was observed in some ELISA results, especially those of A29 and HPV E6 and E7. To reduce this background in the analysed data, we applied a dilution-dependent AUC to represent the antibody titres in Figs. 1d, 6 and 7. The dilution-dependent AUC is a dose-response AUC subtracted from the baseline AUC. The baseline AUC was a product of the $\log_{10}$ dilution span (6.91–2.70 = 4.21) and baseline OD_{450}, which was determined by the average OD_{450} at the past two dilution points ($\log_{10}$ dilutions 6.31 and 6.91). An example of dilution-dependent AUC calculation is provided in the HPV ELISA sections of Source Data Figs. 1–8 and Extended Data Fig. 6, as well as Fig. 7b and Supplementary Fig. 20. Details on antibody titres or AUC values, as well as dilution-dependent AUCs, are summarized in Source Data Figs. 1–8 and Extended Data Fig. 6.

SARS-CoV-2 pseudovirus neutralization assay

A pseudovirus neutralization assay was performed to determine neutralizing antibody titres[51]. Specifically, 1 × 10^4 293T-hACE2 cells were seeded in each well of a 96-well plate 1 d before infection. The next day, plasma collected from mice was serially diluted threefold with complete growth medium at a starting dilution of 1:50. Diluted plasma (55 µl) was mixed with the same volume of SARS-CoV-2 Omicron BA.2.75 or BA.5 variant pseudovirus and incubated at 37 °C for 1 h. After the incubation, 100-µl mixtures were added to 293T-hACE2 cells. The plates were incubated at 37 °C for 20–24 h. Then, cells were trypsinized, washed with MACS buffer once and lysed with Luciferase Cell Culture Lysis (E1531; Promega). The infected cells were quantified using a Nano-Glo Luciferase Assay System (N1120; Promega).

Vaccinia virus lethal challenge experiment in mice

In the lethal challenge experiments, age-matched 8-week-old female BALB/c mice were intramuscularly immunized with two doses of 4 µg MPXVac-097, native or modified A29 and/or M1R LNP mRNAs on days 0 and 7. Vaccinia virus (1 × 10^6 plaque-forming units; Western Reserve strain) was intranasally inoculated into each mouse 2 weeks after the second immunization (day 21; labelled as day 0 after VACV challenge). The mice were monitored every day after challenge for 13 d and the viral infection severity was evaluated by survival rate, weight loss percentage and infection signs. The maximum body weight in the first 3 d after viral challenge was used to normalize the body weight change. The disease score of mice was assigned based on the following criteria: lethargy (score 1); ruffled hair and hunched posture (score 2); weight loss of ≥10% (score 3); and death or weight loss of ≥30% (score 4). Mice were euthanized if they had ≥30% body weight loss. The experiments were conducted in compliance with protocols approved by the Institutional Animal Care and Use Committee at Yale University.

Statistics and reproducibility

Standard statistical methods were applied to the experimental data and are described in the main text, figure captions and Source Data Figs. 1–8 and Extended Data Fig. 6. The data in the dot–bar plots represent means ± s.e.m. and include individual data points. Statistical significance for grouped and ungrouped datasets was determined by two-way analysis of variance with Tukey's or Dunnett's multiple comparisons test and ordinary one-way analysis of variance with Dunnett multiple comparison test, respectively. In certain situations, a pair-wise Tukey's multiple comparison test—the default statistical method in our manuscript—would generate too many asterisks in the graph. To address this issue and highlight the comparisons of interest, such as native antigen versus modified antigens, we used Dunnett's multiple comparison test to determine statistical significance between the control and the other treatment groups in certain plots. The default setting in Prism and two-tailed, unpaired statistical tests were used. No additional adjustments were made for multiple comparisons, unless otherwise stated. Statistically significant comparisons in the figures are respresented by asterisks (*$P < 0.05$; **$P < 0.01$; ***$P < 0.001$; ****$P < 0.0001$). Non-significant comparisons are generally not labelled, but in some instances are denoted by NS. Exact P values are provided in Source Data Figs. 1–8 and Extended Data Fig. 6. Sample numbers are designated as n from biologically independent samples, unless otherwise stated. Sample sizes were determined according to the laboratory's previous work or similar studies in the field[6,51]. Prism (version 10.1.0; GraphPad Software) was used for these analyses.

Reporting summary

Further information on research design is available in the Nature Portfolio Reporting Summary linked to this article.

Data availability

The primary data related to the results of this study can be found within the paper and its Supplementary Information. Source data are provided with this paper.

Code availability

The code used for protein sequence analysis in this study is available on GitHub (https://github.com/fangzhe3/MVP_code)[52].

References

1. August, A. et al. Safety and immunogenicity of an mRNA-based human metapneumovirus and parainfluenza virus type 3 combined vaccine in healthy adults. *Open Forum Infect. Dis.* **9**, ofac206 (2022).
2. John, S. et al. Multi-antigenic human cytomegalovirus mRNA vaccines that elicit potent humoral and cell-mediated immunity. *Vaccine* **36**, 1689–1699 (2018).
3. Awasthi, S. & Friedman, H. M. An mRNA vaccine to prevent genital herpes. *Transl. Res.* **242**, 56–65 (2022).
4. Lee, S. et al. mRNA-HPV vaccine encoding E6 and E7 improves therapeutic potential for HPV-mediated cancers via subcutaneous immunization. *J. Med. Virol.* **95**, e29309 (2023).
5. Zhang, P. et al. A multiclade *env–gag* VLP mRNA vaccine elicits tier-2 HIV-1-neutralizing antibodies and reduces the risk of heterologous SHIV infection in macaques. *Nat. Med.* **27**, 2234–2245 (2021).
6. Fang, Z. et al. Polyvalent mRNA vaccination elicited potent immune response to monkeypox virus surface antigens. *Cell Res.* **33**, 407–410 (2023).
7. Monslow, M. A. et al. Immunogenicity generated by mRNA vaccine encoding VZV gE antigen is comparable to adjuvanted subunit vaccine and better than live attenuated vaccine in nonhuman primates. *Vaccine* **38**, 5793–5802 (2020).
8. Essink, B. et al. The safety and immunogenicity of two Zika virus mRNA vaccine candidates in healthy flavivirus baseline seropositive and seronegative adults: the results of two randomised, placebo-controlled, dose-ranging, phase 1 clinical trials. *Lancet Infect. Dis.* **23**, 621–633 (2023).
9. Barbier, A. J., Jiang, A. Y., Zhang, P., Wooster, R. & Anderson, D. G. The clinical progress of mRNA vaccines and immunotherapies. *Nat. Biotechnol.* **40**, 840–854 (2022).
10. Pardi, N., Hogan, M. J., Porter, F. W. & Weissman, D. mRNA vaccines—a new era in vaccinology. *Nat. Rev. Drug Discov.* **17**, 261–279 (2018).
11. Freed, D. C. et al. Pentameric complex of viral glycoprotein H is the primary target for potent neutralization by a human cytomegalovirus vaccine. *Proc. Natl Acad. Sci. USA* **110**, E4997–E5005 (2013).
12. He, Y. et al. Antibodies to the A27 protein of vaccinia virus neutralize and protect against infection but represent a minor component of Dryvax vaccine-induced immunity. *J. Infect. Dis.* **196**, 1026–1032 (2007).
13. Kaever, T. et al. Linear epitopes in vaccinia virus A27 are targets of protective antibodies induced by vaccination against smallpox. *J. Virol.* **90**, 4334–4345 (2016).
14. Li, M. et al. Three neutralizing mAbs induced by MPXV A29L protein recognizing different epitopes act synergistically against orthopoxvirus. *Emerg. Microbes Infect.* **12**, 2223669 (2023).
15. Xia, H., He, Y. R., Zhan, X. Y. & Zha, G. F. Mpox virus mRNA-lipid nanoparticle vaccine candidates evoke antibody responses and drive protection against the vaccinia virus challenge in mice. *Antivir. Res.* **216**, 105668 (2023).
16. Kreiter, S. et al. Mutant MHC class II epitopes drive therapeutic immune responses to cancer. *Nature* **520**, 692–696 (2015).
17. Ramos da Silva, J. et al. Single immunizations of self-amplifying or non-replicating mRNA-LNP vaccines control HPV-associated tumors in mice. *Sci. Transl. Med.* **15**, eabn3464 (2023).
18. Harper, D. M. et al. Efficacy of a bivalent L1 virus-like particle vaccine in prevention of infection with human papillomavirus types 16 and 18 in young women: a randomised controlled trial. *Lancet* **364**, 1757–1765 (2004).
19. Tan, M. Norovirus vaccines: current clinical development and challenges. *Pathogens* **10**, 1641 (2021).
20. Dattwyler, R. J. & Gomes-Solecki, M. The year that shaped the outcome of the OspA vaccine for human Lyme disease. *npj Vaccines* **7**, 10 (2022).
21. Bonam, S. R., Renia, L., Tadepalli, G., Bayry, J. & Kumar, H. M. S. Plasmodium falciparum malaria vaccines and vaccine adjuvants. *Vaccines* **9**, 1072 (2021).
22. Polack, F. P. et al. Safety and efficacy of the BNT162b2 mRNA COVID-19 vaccine. *N. Engl. J. Med.* **383**, 2603–2615 (2020).
23. Baden, L. R. et al. Efficacy and safety of the mRNA-1273 SARS-CoV-2 vaccine. *N. Engl. J. Med.* **384**, 403–416 (2021).
24. Fang, Z. et al. Heterotypic vaccination responses against SARS-CoV-2 Omicron BA.2. *Cell Discov.* **8**, 69 (2022).
25. Sample, P. J. et al. Human 5′ UTR design and variant effect prediction from a massively parallel translation assay. *Nat. Biotechnol.* **37**, 803–809 (2019).
26. Leppek, K. et al. Combinatorial optimization of mRNA structure, stability, and translation for RNA-based therapeutics. *Nat. Commun.* **13**, 1536 (2022).
27. Cao, J. et al. High-throughput 5′ UTR engineering for enhanced protein production in non-viral gene therapies. *Nat. Commun.* **12**, 4138 (2021).
28. Henderson, J. M. et al. Cap 1 messenger RNA synthesis with co-transcriptional CleanCap® analog by in vitro transcription. *Curr. Protoc.* **1**, e39 (2021).

29. Kariko, K., Buckstein, M., Ni, H. & Weissman, D. Suppression of RNA recognition by Toll-like receptors: the impact of nucleoside modification and the evolutionary origin of RNA. *Immunity* **23**, 165–175 (2005).
30. Hoffmann, M. A. G. et al. ESCRT recruitment to SARS-CoV-2 spike induces virus-like particles that improve mRNA vaccines. *Cell* **186**, 2380–2391.e9 (2023).
31. Berger, A. Th1 and Th2 responses: what are they? *Br. Med. J.* **321**, 424 (2000).
32. Romagnani, S. T-cell subsets (Th1 versus Th2). *Ann. Allergy Asthma Immunol.* **85**, 9–18 (2000).
33. Cheng, X. et al. A synergistic lipid nanoparticle encapsulating mRNA shingles vaccine induces potent immune responses and protects guinea pigs from viral challenges. *Adv. Mater.* **36**, e2310886 (2024).
34. Tao, M., Kruhlak, M., Xia, S., Androphy, E. & Zheng, Z. M. Signals that dictate nuclear localization of human papillomavirus type 16 oncoprotein E6 in living cells. *J. Virol.* **77**, 13232–13247 (2003).
35. Verbeke, R., Hogan, M. J., Lore, K. & Pardi, N. Innate immune mechanisms of mRNA vaccines. *Immunity* **55**, 1993–2005 (2022).
36. Akkaya, M., Kwak, K. & Pierce, S. K. B cell memory: building two walls of protection against pathogens. *Nat. Rev. Immunol.* **20**, 229–238 (2020).
37. Rock, K. L., Reits, E. & Neefjes, J. Present yourself! By MHC class I and MHC class II molecules. *Trends Immunol.* **37**, 724–737 (2016).
38. Kreiter, S. et al. Increased antigen presentation efficiency by coupling antigens to MHC class I trafficking signals. *J. Immunol.* **180**, 309–318 (2008).
39. Arieta, C. M. et al. The T-cell-directed vaccine BNT162b4 encoding conserved non-spike antigens protects animals from severe SARS-CoV-2 infection. *Cell* **186**, 2392–2409.e21 (2023).
40. Zuiani, A. et al. A multivalent mRNA monkeypox virus vaccine (BNT166) protects mice and macaques from orthopoxvirus disease. *Cell* **187**, 1363–1373.e12 (2024).
41. Weber, J. S. et al. Individualised neoantigen therapy mRNA-4157 (V940) plus pembrolizumab versus pembrolizumab monotherapy in resected melanoma (KEYNOTE-942): a randomised, phase 2b study. *Lancet* **403**, 632–644 (2024).
42. Rojas, L. A. et al. Personalized RNA neoantigen vaccines stimulate T cells in pancreatic cancer. *Nature* **618**, 144–150 (2023).
43. Cafri, G. et al. mRNA vaccine-induced neoantigen-specific T cell immunity in patients with gastrointestinal cancer. *J. Clin. Invest.* **130**, 5976–5988 (2020).
44. Moffat, J. et al. Functions of the C-terminal domain of varicella-zoster virus glycoprotein E in viral replication in vitro and skin and T-cell tropism in vivo. *J. Virol.* **78**, 12406–12415 (2004).
45. Barash, S., Wang, W. & Shi, Y. Human secretory signal peptide description by hidden Markov model and generation of a strong artificial signal peptide for secreted protein expression. *Biochem. Biophys. Res. Commun.* **294**, 835–842 (2002).
46. Dai, X. et al. One-step generation of modular CAR-T cells with AAV–Cpf1. *Nat. Methods* **16**, 247–254 (2019).
47. Reiss, S. et al. Comparative analysis of activation induced marker (AIM) assays for sensitive identification of antigen-specific CD4 T cells. *PLoS ONE* **12**, e0186998 (2017).
48. Galvez, R. I. et al. Frequency of Dengue virus-specific T cells is related to infection outcome in endemic settings. *JCI Insight* **10**, e179771 (2025).
49. Peng, L. et al. Variant-specific vaccination induces systems immune responses and potent in vivo protection against SARS-CoV-2. *Cell Rep. Med.* **3**, 100634 (2022).
50. Ye, L. et al. A genome-scale gain-of-function CRISPR screen in CD8 T cells identifies proline metabolism as a means to enhance CAR-T therapy. *Cell Metab.* **34**, 595–614.e14 (2022).
51. Fang, Z. et al. Omicron-specific mRNA vaccination alone and as a heterologous booster against SARS-CoV-2. *Nat. Commun.* **13**, 3250 (2022).
52. Fang, Z. et al. fangzhe3 / MVP_code. *GitHub* https://github.com/fangzhe3/MVP_code (2025).

Acknowledgements

This work was supported by discretionary funds and a Cancer Research Institute Lloyd J. Old STAR Award (CRI4964) to S.C. We acknowledge support from various Yale core facilities: the Systems Biology Institute, Department of Genetics, Department of Immunobiology, Yale School of Medicine Dean's Office and Office of the Vice Provost for Research. We thank X. Chen, L. Chen, F. Fenteany, L. Lawres, L. Zhou, K. Tang, X. Zhou, P. Ren and many other laboratory members and/or colleagues for providing reagents, suggestions and technical assistance. Z. Fang is supported by the Canadian Institutes of Health Research (funding reference number 194053).

Author contributions

S.C. conceived of the study and designed it with Z.F. Z.F. performed most of the experiments and analysed the data. V.S.M. performed the VACV challenge experiment. C.O. prepared the HPV-transduced cell lines. K.A.J., L.R. and N.A. assisted with the experiments related to molecular cloning, ELISA and flow cytometry. L.Y. and L.P. conducted the experiments involving lentivirus production and transduction. Z.F., D.D., C.L. and S.C. wrote the paper with input from all authors. C.L. and S.C. supervised the study.

Competing interests

S.C. is a (co)founder of EvolveImmune Therapeutics, Cellinfinity Bio, MagicTime Medicine and Chen Consulting, all unrelated to this study. A patent application related to this study has been filed by Yale University. The patent titled 'Compositions and Methods for Enhancement of mRNA Vaccine Performance and Vaccination Against Mpox' (PCT International Appl. No. PCT/US2023/081090) covers the related biotechnology. The other authors declare no competing interests.

Additional information

Extended data is available for this paper at https://doi.org/10.1038/s41551-025-01478-6.

Supplementary information The online version contains supplementary material available at https://doi.org/10.1038/s41551-025-01478-6.

Correspondence and requests for materials should be addressed to Carolina Lucas or Sidi Chen.

Peer review information *Nature Biomedical Engineering* thanks Anna Blakney and the other, anonymous, reviewer(s) for their contribution to the peer review of this work. Peer reviewer reports are available.

https://doi.org/10.1038/s41551-025-01478-6

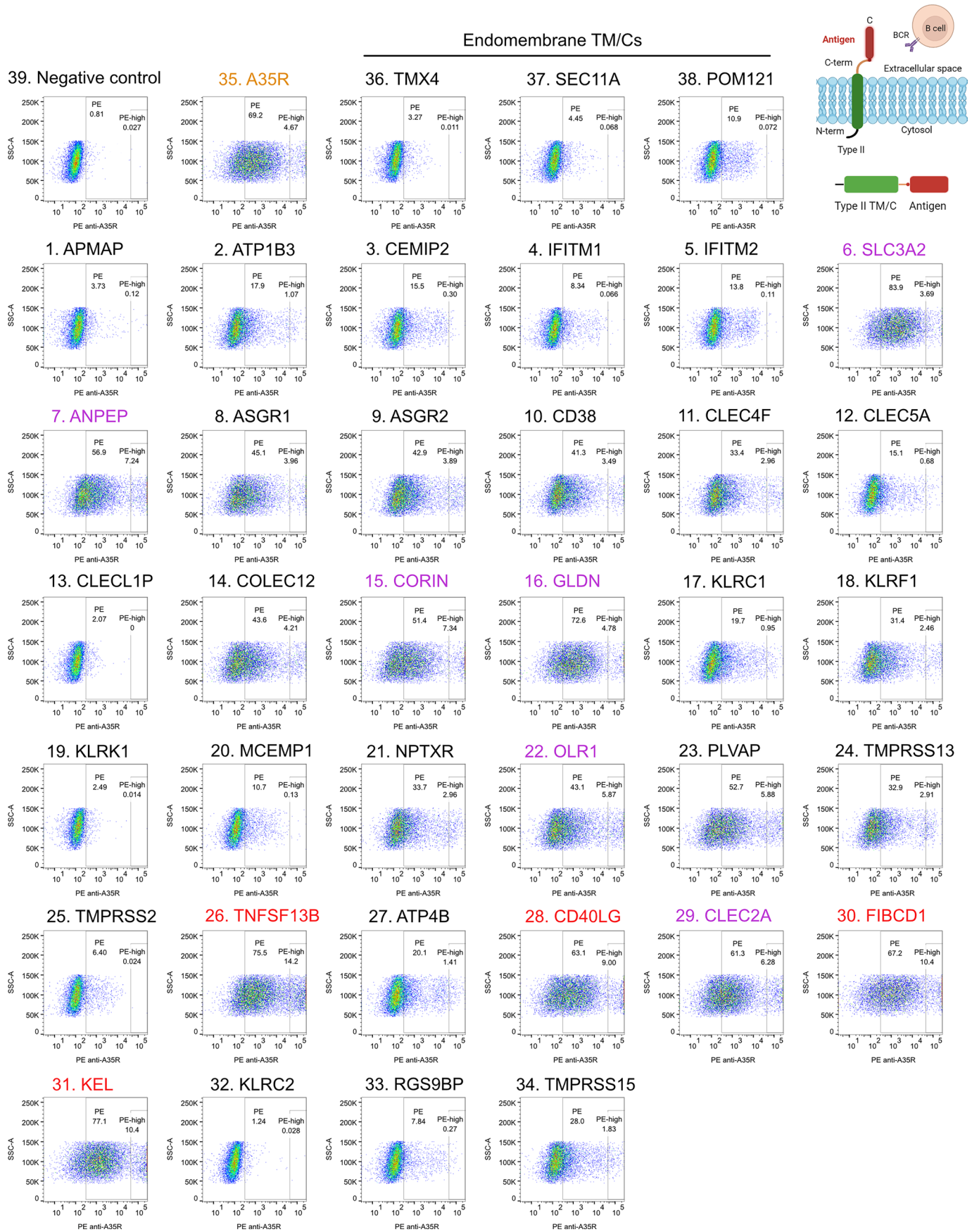

Extended Data Fig. 1 | See next page for caption.

https://doi.org/10.1038/s41551-025-01478-6

Extended Data Fig. 1 | Flow cytometry gating strategy to select A35R-positive 293T cells which overexpressed A35R ectodomain recombined with various N-term type II TM/Cs and were surface stained with PE anti-A35R antibody. The 293T cells were gated at low and high threshold to define PE and PE-high populations, respectively (n = 3). The A35R TM/C + A35R ectodomain served as the internal control. The A35R ectodomains with endomembrane protein TM/Cs, such as TMX4, SEC11A, PM121, served as TM/C negative controls. The TM/C modules that outperformed A35R TM/C (orange) are highlighted in red or purple (color based on their located quadrants in Fig. 2a). Schematic (top right) created with BioRender.com.

https://doi.org/10.1038/s41551-025-01478-6

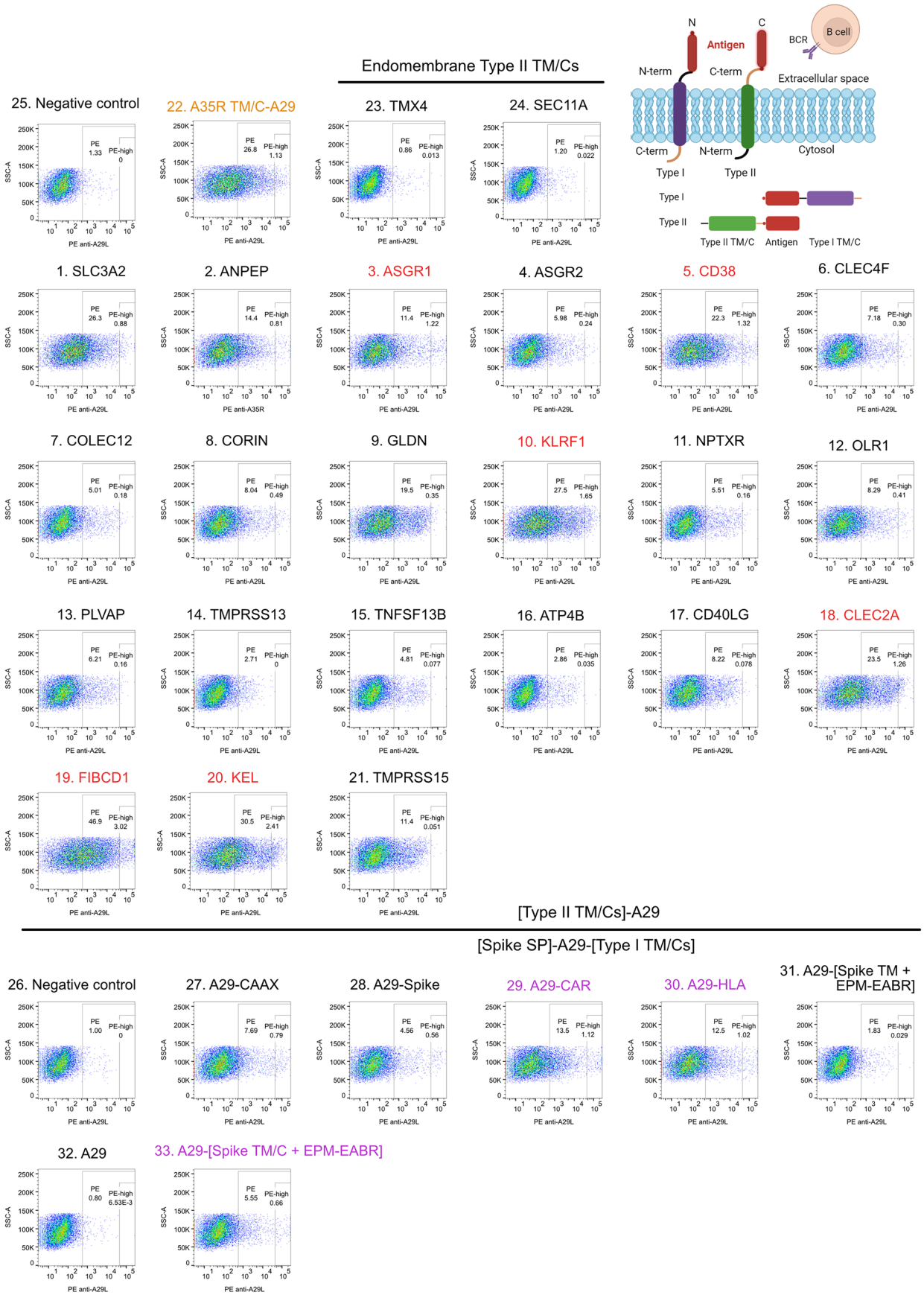

Extended Data Fig. 2 | See next page for caption.

https://doi.org/10.1038/s41551-025-01478-6

Extended Data Fig. 2 | Representative flow plots showing the gating strategies to define PE or PE-high positive 293T cells that overexpressed A29 with or without either [Spike SP] + type I TM/Cs (bottom panel) or Type II TM/Cs (top panel) and were surface stained with PE anti-A29 antibody. The A35R TM/C + A29 served as the internal control, while the A29 with endomembrane protein type II TM/Cs, including TMX4 and SEC11A, served as TM/C negative controls. The TM/C modules that outperformed A35R TM/C (orange) are highlighted in red or purple (color based on their type I or type II topology). Schematic (top right) created with BioRender.com.

https://doi.org/10.1038/s41551-025-01478-6

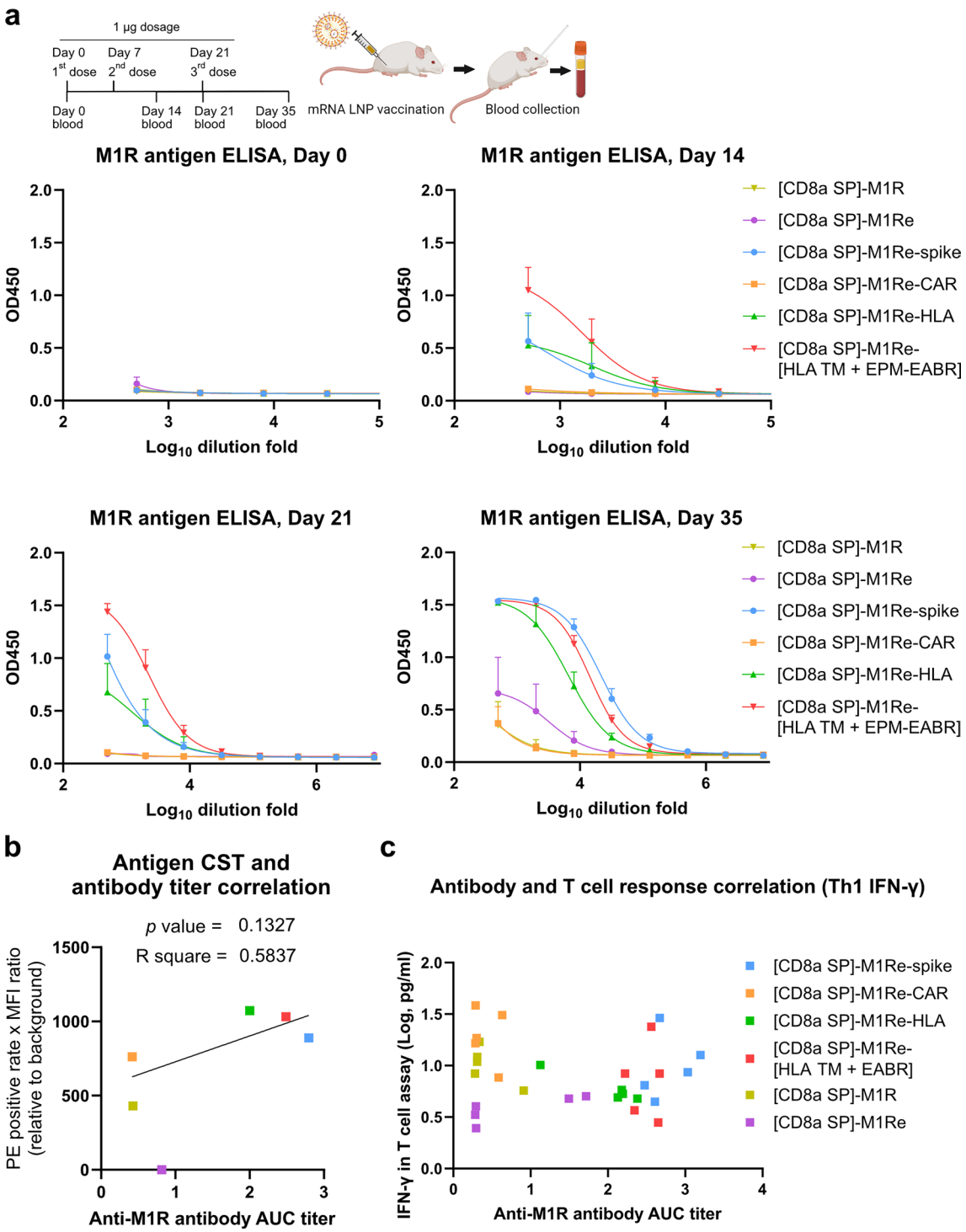

Extended Data Fig. 3 | ELISA titration curves over serial dilutions of plasma collected on different days from mice immunized with 1 μg [CD8 SP]-M1Re LNP-mRNAs with different TM/Cs. a, ELISA titration curves on days 0, 14, 21 and 35 (n = 5). The immunization schedule is shown at the top of the graph. **b**, correlation of antibody titers against M1R with corresponding antigen's expression on 293T cells. The antigen expression as CST quantified by normalized PE integral (positive rate x positive MFI ratio) is plotted against anti-M1R antibody AUC titer. all data points except for the secreted M1Re is analyzed in linear regression. **c**, TM/C modules modulated the antibody and T cell response to LNP-mRNA of chimeric [CD8a SP]-M1Re in mice. The anti-M1R antibody titer on day 35 is plotted against Th1 response (IFN- γ as an indicator). Data are presented as mean ± SEM. Schematic in **a** created with BioRender.com.

https://doi.org/10.1038/s41551-025-01478-6

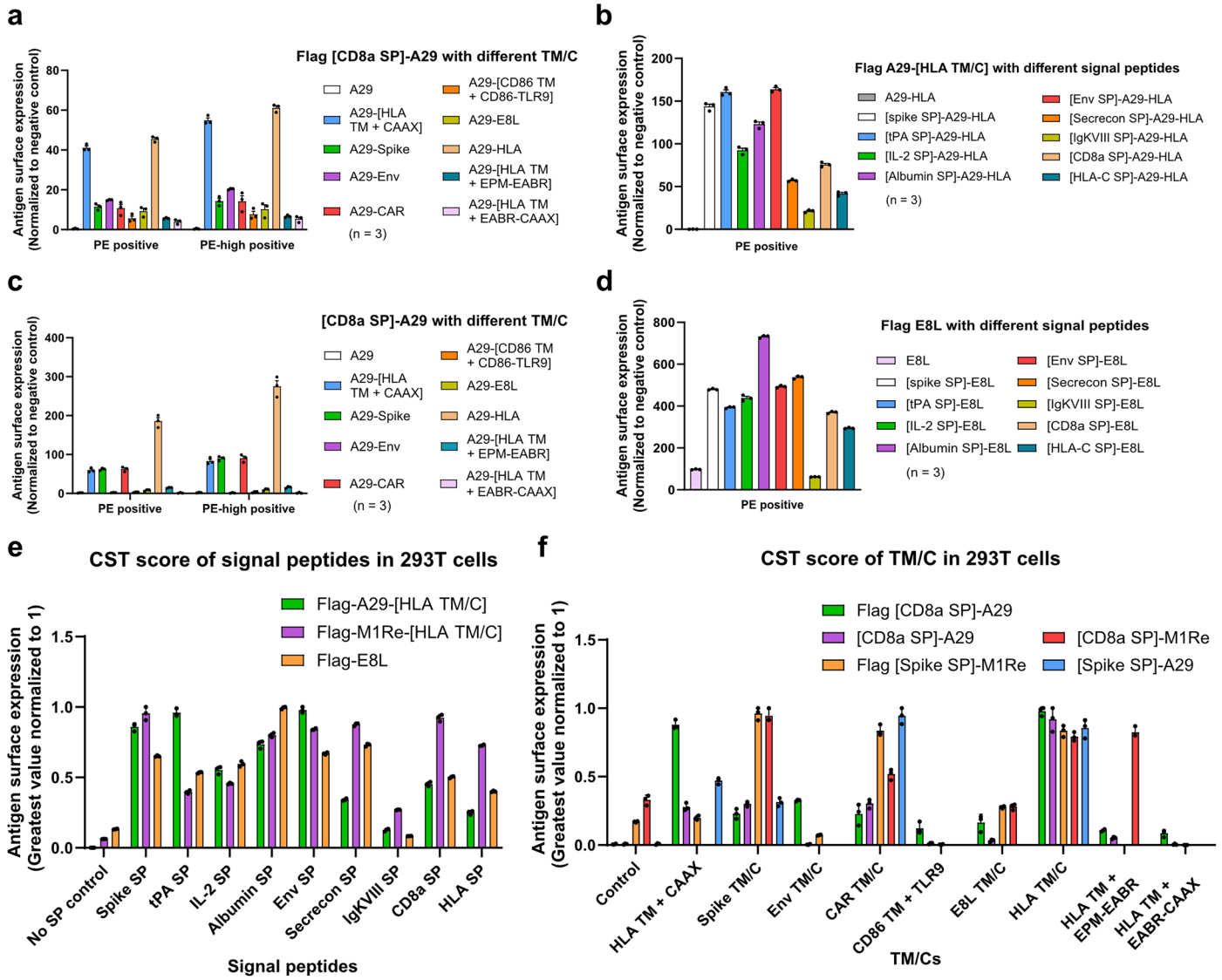

Extended Data Fig. 4 | The CST scores were calculated from normalized antigen surface expression and were used to evaluate SP and TM/C modules' strength to promote different Mpox antigens translocation to cell surface. **a,c**, The fusion of flag-tagged (**a**) or untagged (**c**) [CD8a SP]-A29 with different type I TM/Cs enhanced its surface expression in 293T cells (n = 3). **b,d**, Various N-term signal peptides increased flag tagged A29-[HLA TM/C] (**b**) or E8L (**d**) surface expression levels (n = 3). **e,f**, The CST score was used to evaluate the signal strength of different SP (**e**) or TM/C (**f**) modules at promoting antigen expression on 293T cell surface. It is derived from normalized antigen expression, of which largest value in each dataset was normalized to 1. **e**, Various signal peptides (SP) increased cell-surface expression of flag-tagged Mpox antigens, including A29, M1Re and E8L (n = 3). **f**, Different type I TM/Cs improved cell-surface expression of flag-tagged or untagged A29 and M1Re in 293 T cells (n = 3). Data are presented as mean ± SEM.

https://doi.org/10.1038/s41551-025-01478-6

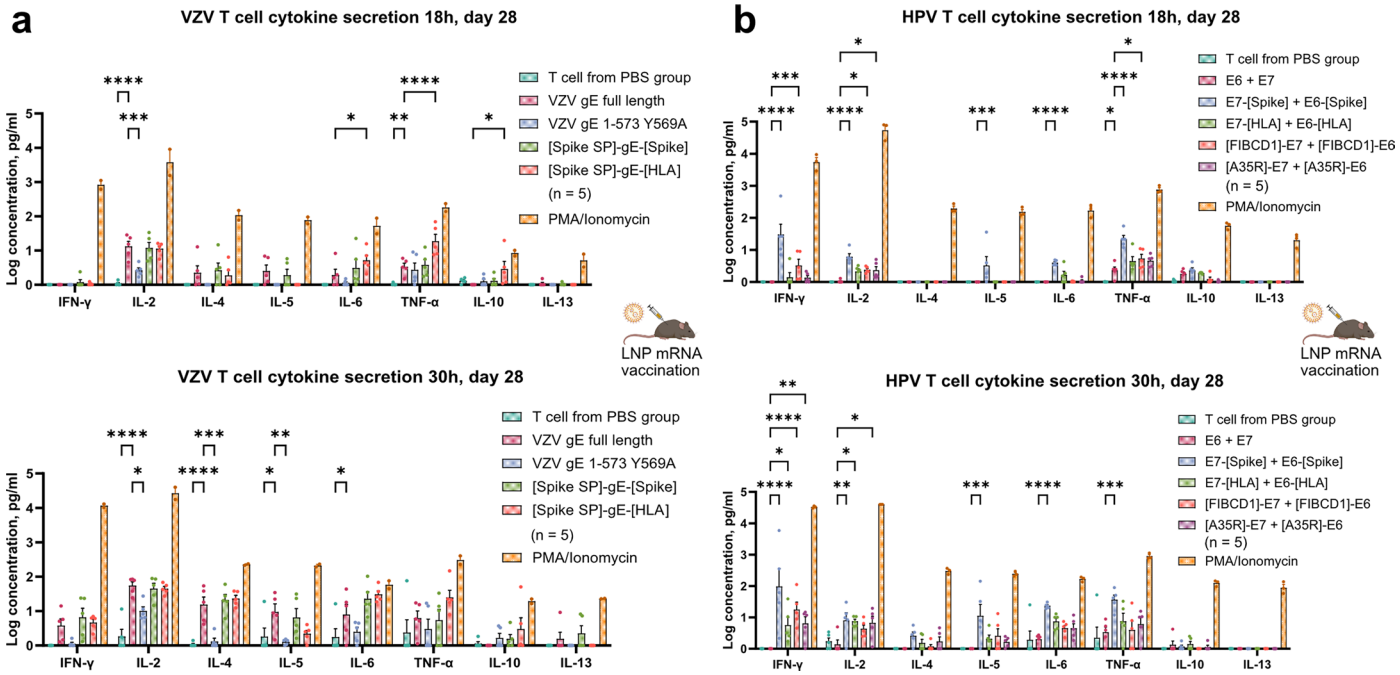

Extended Data Fig. 5 | T cells from mice vaccinated with MVP-modified mRNA antigens showed higher cytokine secretion after VZV or HPV antigen stimulation. PBMCs were collected on day 28 from mice vaccinated different LNP mRNAs and stimulated with VZV gE antigen or HPV E6, E7 peptides for 18 and 30 hours. The secreted cytokines in media were measured by beads-based immunoassays (seen methods). **a**, Cytokine secretion of T cells stimulated with VZV gE antigen for 18 h (top) and 30 h (bottom). **b**, Cytokine secretion of T cells stimulated with HPV E6 and E7 scanning peptide pools for 18 h (top) and 30 h (bottom). All statistics were derived from Dunnett's multiple comparison test between controls (VZV gE full length or HPV16 E6 + E7) and other treatment groups. PMA/Ionomycin group was excluded from comparisons. Sample number of vaccination groups (except for PMA/Ionomycin) is 5. Data are presented as mean ± SEM. Dunnett's comparison test was used to determine statistical significance between WT antigens and modified antigen groups. * $p < 0.05$, ** $p < 0.01$, *** $p < 0.001$, **** $p < 0.0001$. Mouse icons created with BioRender.com.

https://doi.org/10.1038/s41551-025-01478-6

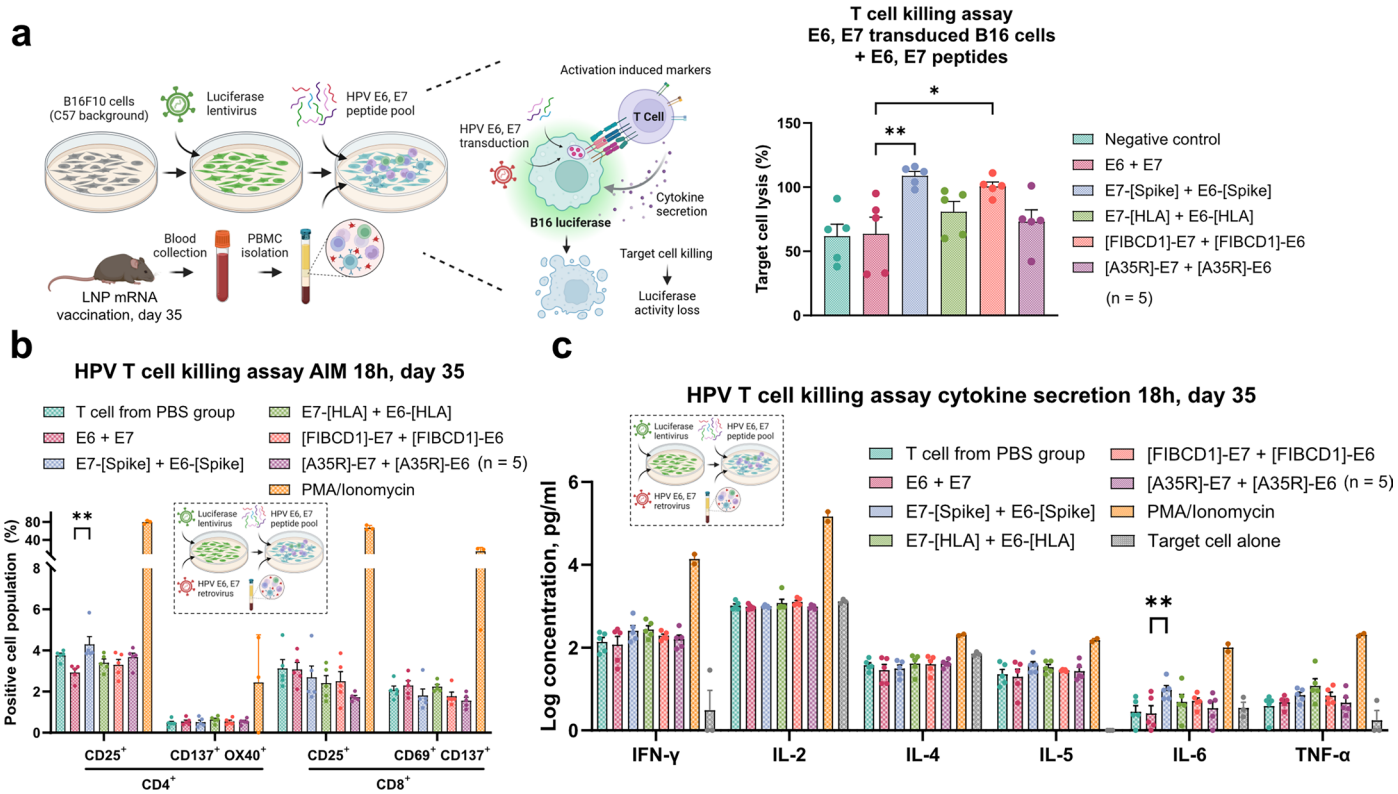

Extended Data Fig. 6 | Compared to E6 + E7 vaccination control, T cells collected on day 35 from mice vaccinated with MVP-modified E6 and E7 mRNA antigens showed higher target cell killing activity (a), activation induced markers (b) and cytokine secretion (c) after 18-hour co-culture with B16F10 target cells transduced with HPV16 wild-type E6 + E7 and pulsed with E6, E7 peptides. a, T cells from mice vaccinated with MVP-modified E6, E7 mRNA antigens led to higher cytolysis of B16F10 target cells (n = 5). **b**, Activation induced markers were surface stained in T cells from different LNP mRNA vaccination groups after co-culture with target cells (n = 5). **c**, Cytokine secretion of T cells co-cultured with target cells for 18 hours (n = 5). The secreted cytokines in media were measured by beads-based immunoassays (seen methods). Target cell alone showed baseline levels of cytokines in media. Additional cytokines, such as IL-2 and IL-12 were added to media to maintain effector function of T cells. All statistics were derived from Dunnett's multiple comparison test between HPV16 E6 + E7 and other treatment groups. PMA/Ionomycin group was excluded from comparisons. Sample number of vaccination groups is 5, except for PMA/Ionomycin and target cell. Data are presented as mean ± SEM. Dunnett's comparison test was used to determine statistical significance between WT antigens and modified antigen groups. * $p < 0.05$, ** $p < 0.01$, *** $p < 0.001$, **** $p < 0.0001$. Panel **a** and insets in **b** and **c** created with BioRender.com.

nature research

Corresponding author(s): Sidi Chen

Last updated by author(s): May 20, 2025

Reporting Summary

Nature Research wishes to improve the reproducibility of the work that we publish. This form provides structure for consistency and transparency in reporting. For further information on Nature Research policies, see Authors & Referees and the Editorial Policy Checklist.

Statistics

For all statistical analyses, confirm that the following items are present in the figure legend, table legend, main text, or Methods section.

n/a	Confirmed
☐	☒ The exact sample size (*n*) for each experimental group/condition, given as a discrete number and unit of measurement
☐	☒ A statement on whether measurements were taken from distinct samples or whether the same sample was measured repeatedly
☐	☒ The statistical test(s) used AND whether they are one- or two-sided *Only common tests should be described solely by name; describe more complex techniques in the Methods section.*
☐	☒ A description of all covariates tested
☐	☒ A description of any assumptions or corrections, such as tests of normality and adjustment for multiple comparisons
☐	☒ A full description of the statistical parameters including central tendency (e.g. means) or other basic estimates (e.g. regression coefficient) AND variation (e.g. standard deviation) or associated estimates of uncertainty (e.g. confidence intervals)
☐	☒ For null hypothesis testing, the test statistic (e.g. *F*, *t*, *r*) with confidence intervals, effect sizes, degrees of freedom and *P* value noted *Give P values as exact values whenever suitable.*
☒	☐ For Bayesian analysis, information on the choice of priors and Markov chain Monte Carlo settings
☒	☐ For hierarchical and complex designs, identification of the appropriate level for tests and full reporting of outcomes
☒	☐ Estimates of effect sizes (e.g. Cohen's *d*, Pearson's *r*), indicating how they were calculated

Our web collection on statistics for biologists contains articles on many of the points above.

Software and code

Policy information about availability of computer code

Data collection	Default softwares in the data collection instruments including Attune focusing cytometer (Attune NxT Software v3.1), BD FACSAria III Cell Sorter and PerkinElmer EnVision 2105 microplate reader (Envision Manager v1.13.3009.1401) were used to collect data. All data are summarized in the excel file named, 20250205_data_summary_v23.
Data analysis	Data analysis were performed using Prism (version 10.1.0, GraphPad Software Inc.) for small scale data analysis. The code used for protein sequence analysis in this study is available from GitHub (https://github.com/fangzhe3/MVP_code).

For manuscripts utilizing custom algorithms or software that are central to the research but not yet described in published literature, software must be made available to editors/reviewers. We strongly encourage code deposition in a community repository (e.g. GitHub). See the Nature Research guidelines for submitting code & software for further information.

Data

Policy information about availability of data

All manuscripts must include a data availability statement. This statement should provide the following information, where applicable:

- Accession codes, unique identifiers, or web links for publicly available datasets
- A list of figures that have associated raw data
- A description of any restrictions on data availability

The primary data related to the results of this study can be found within the paper and its supplementary information. The statistical details required to recreate the figures are included as Source Data. The source data generated during the study are provided within this paper and its supplementary excel file.

Field-specific reporting

Please select the one below that is the best fit for your research. If you are not sure, read the appropriate sections before making your selection.

☒ Life sciences ☐ Behavioural & social sciences ☐ Ecological, evolutionary & environmental sciences

For a reference copy of the document with all sections, see nature.com/documents/nr-reporting-summary-flat.pdf

Life sciences study design

All studies must disclose on these points even when the disclosure is negative.

Sample size	For most cases, each group has at least three biologically independent samples unless otherwise noted. Details on sample size for each experiment were indicated in methods and figure legends. Sample size was determined according to the lab's prior work or similar studies in the field.
Data exclusions	No data were excluded in this study.
Replication	Biological replicates of mice and flow cytometry samples were collected in each experiment.
Randomization	Mice were randomly allocated into experimental or control groups. For all experiments not involving mice, sample allocation into experimental groups was performed based on predefined experimental conditions rather than by randomization. In cases where randomization was not feasible, we ensured balance across key covariates (e.g., treatment duration, transfection plasmid amount) by evenly distributing samples based on these factors to minimize potential confounding. For studies where group allocation was not applicable, the question of allocation did not arise and is therefore not relevant.
Blinding	Blinding was not used in this study. Blinding was not employed in this study because the experimental procedures and data analyses were conducted using quantitative readouts and standardized protocols (e.g., flow cytometry, ELISA) that are not subject to or have minimal risk of observer bias.

Reporting for specific materials, systems and methods

We require information from authors about some types of materials, experimental systems and methods used in many studies. Here, indicate whether each material, system or method listed is relevant to your study. If you are not sure if a list item applies to your research, read the appropriate section before selecting a response.

Materials & experimental systems

n/a	Involved in the study
☐	☒ Antibodies
☐	☒ Eukaryotic cell lines
☒	☐ Palaeontology
☐	☒ Animals and other organisms
☒	☐ Human research participants
☒	☐ Clinical data

Methods

n/a	Involved in the study
☒	☐ ChIP-seq
☐	☒ Flow cytometry
☒	☐ MRI-based neuroimaging

Antibodies

Antibodies used

1. HRP-conjugated anti-mouse IgG (H+L) antibody (Fisher, Cat. No. A16072, 1:2500 dilution)
2. PE-conjugated anti-mouse IgG (H+L) antibody (Fisher, Cat. No. P-852, 1:100 dilution)
3. PE-conjugated anti-flag antibody (BioLegend, 637310, 1:100 dilution)
4. Anti-A35R antibody (Sino Biological, 40886-M0026-100, 1:100 dilution)
5. Anti-M1R antibody (Cell Sciences RVV13901B or Innovative Research IMSAVACVL1R7D11C100UG, 1:100 dilution)
6. Anti-A29L antibody (Sino Biological 40891-M0032-100, 1:100 dilution)
7. Anti-VZV gE antibody (Sino Biological, 40907-MM12, 1:100 dilution)
8. Anti-HPV16/18 E6 with FITC fluorophore (Santa Cruz biotechnology, sc-460 FITC, 1:100 dilution)
9. Anti-HPV16 E7 with PE fluorophore (Santa Cruz biotechnology, sc-6981 PE, 1:100 dilution)
10. Anti-CD3 PE/Cy7 (Biolegend, Clone 17A2, 1:100 dilution)
11. Anti-CD8a BV421 (Biolegend, Clone QA17A07, 1:100 dilution)
12. Anti-CD4 FITC (Biolegend, Clone GK1.5, 1:100 dilution)
13. Anti-CD25 BV650 (Biolegend, Clone PC61, 1:100 dilution)
14. Anti-CD69 APC/Cy7 (Biolegend, Clone H1.2F3, 1:100 dilution)
15. Anti-CD137 PE (Biolegend, Clone 17B5, 1:50 dilution)
16. Anti-CD134 PerCP/Cy5.5 (OX40, Biolegend, Clone OX-86, 1:50 dilution)
17. Anti-IFN-γ PE (Biolegend, Clone W18272D,1:100 dilution)
18. Anti-TNF-α Percp-Cy5.5 (Biolegend, Clone MP6-XT22, 1:100 dilution)

19. Anti-IL-2 BV510 (Biolegend, Clone JES6-5H4, 1:100 dilution)
20. Anti-IL-4 BV605 (Biolegend, Clone 11B11,1:100 dilution)
21. Anti-IL-5 APC(Biolegend, Clone TRFK5,1:100 dilution)

Validation

Commercial antibodies were validated by the vendors, and re-validated in house as appropriate through antigen-specific experiments. Commercial antibody info and validation info where applicable:
1. HRP-conjugated anti-mouse IgG (H+L) antibody (Fisher, Cat. No. A16072, 1:2500 dilution): Goat anti-Mouse IgG (H+L) Cross-Adsorbed, HRP (A16072) (thermofisher.com)
2. PE-conjugated anti-mouse IgG (H+L) antibody (Fisher, Cat. No. P-852, 1:100 dilution): Goat anti-Mouse IgG (H+L) Cross-Adsorbed, PE (P-852) (thermofisher.com)
3. PE-conjugated anti-flag antibody (BioLegend, 637310): https://www.biolegend.com/nl-nl/products/pe-anti-dykddddk-tag-antibody-9383?GroupID=GROUP26
4. Anti-A35R antibody (Sino Biological, 40886-M0026-100): https://www.sinobiological.com/antibodies/protein-a35-40886-m0026
5. Anti-M1R antibody (Cell Sciences RVV13901B or Innovative Research IMSAVACVL1R7D11C100UG): https://www.cellsciences.com/mouse-anti-vaccinia-l1r-protein-l1-antibody-7d11
6. Anti-A29L antibody (Sino Biological 40891-M0032-100): https://www.sinobiological.com/antibodies/protein-a29-40891-m0032
7. Anti-VZV gE antibody (Sino Biological, 40907-MM12): https://www.sinobiological.com/antibodies/ge-40907-mm12
8. Anti-HPV16/18 E6 with FITC fluorophore (Santa Cruz biotechnology, sc-460 FITC): https://www.scbt.com/p/hpv16-e6-18-e6-antibody-c1p5?srsltid=AfmBOop3TBSPTztjsvQ3lkyy_eLMJRNAOrtV1VD6aJCAEQj_yylZPHex
9. AAnti-HPV16 E7 with PE fluorophore (Santa Cruz biotechnology, sc-6981 PE): https://www.scbt.com/p/hpv16-e7-antibody-ed17?srsltid=AfmBOopnjrAjMSV3iSWETnGHkRME7iZ8VwIOpzQZtL1dpyyTxEcbqGbS
10. Anti-CD3 PE/Cy7 (Biolegend, Clone 17A2, 1:100 dilution): https://www.biolegend.com/en-ie/products/pe-cyanine7-anti-mouse-cd3-antibody-6060
11. Anti-CD8a BV421 (Biolegend, Clone QA17A07, 1:100 dilution): https://www.biolegend.com/nl-nl/products/brilliant-violet-421-anti-mouse-cd8a-recombinant-antibody-18186
12. Anti-CD4 FITC (Biolegend, Clone GK1.5, 1:100 dilution): https://www.biolegend.com/fr-lu/products/fitc-anti-mouse-cd4-antibody-248
13. Anti-CD25 BV650 (Biolegend, Clone PC61, 1:100 dilution): https://www.biolegend.com/nl-be/products/brilliant-violet-650-anti-mouse-cd25-antibody-7640
14. Anti-CD69 APC/Cy7 (Biolegend, Clone H1.2F3, 1:100 dilution): https://www.biolegend.com/en-gb/products/apc-cyanine7-anti-mouse-cd69-antibody-6986?GroupID=BLG10536
15. Anti-CD137 PE (Biolegend, Clone 17B5, 1:50 dilution): https://www.biolegend.com/ja-jp/products/pe-anti-mouse-cd137-antibody-51
16. Anti-CD134 PerCP/Cy5.5 (OX40, Biolegend, Clone OX-86, 1:50 dilution): https://www.biolegend.com/fr-ch/products/percp-cyanine5-5-anti-mouse-cd134-ox-40-antibody-14846
17. Anti-IFN-γ PE (Biolegend, Clone W18272D,1:100): https://www.biolegend.com/fr-ch/products/pe-anti-mouse-ifn-gamma-antibody-20614
18. Anti-TNF-α Percp-Cy5.5 (Biolegend, Clone MP6-XT22, 1:100): https://www.biolegend.com/en-ie/products/percp-cyanine5-5-anti-mouse-tnf-alpha-antibody-4438
19. Anti-IL-2 BV510 (Biolegend, Clone JES6-5H4, 1:100): https://www.biolegend.com/fr-ch/products/brilliant-violet-510-anti-mouse-il-2-antibody-9274
20. Anti-IL-4 BV605 (Biolegend, Clone 11B11,1:100): https://www.biolegend.com/en-gb/products/brilliant-violet-605-anti-mouse-il-4-antibody-8534
21. Anti-IL-5 APC (Biolegend, Clone TRFK5,1:100): https://www.biolegend.com/en-gb/products/apc-anti-mouse-human-il-5-antibody-989

Eukaryotic cell lines

Policy information about cell lines

Cell line source(s)

Commercial cell lines HEK293T (CRL-3216), RAW264.7 (TIB-71) and B16F10 (CRL-6475) were originally acquired from ATCC and maintained by members in Chen lab. The DC2.4 cell line was a generous gift from Dr. Lieping Chen lab at Yale University.

Authentication

Cell lines were authenticated by original vendors, and re-validated in lab as appropriate by morphology.

Mycoplasma contamination

All cell lines were tested negative for mycoplasma contamination.

Commonly misidentified lines
(See ICLAC register)

No misidentified cell lines were used in the study.

Animals and other organisms

Policy information about studies involving animals; ARRIVE guidelines recommended for reporting animal research

Laboratory animals

C57BL/6Ncr (B6) mice and BALB/c mice, female 7-10 week mice were purchased from Charles River.

Wild animals

No wild animals were used in the study.

Field-collected samples

No field collected samples were used in the study.

Ethics oversight

Both recombinant DNA (rDNA) and biosafety work were conducted following the guidelines of Yale Environment, Health and

Ethics oversight	Safety (EHS) Committee with approved protocols (Chen 18–45, 20–18, and 20–26). All animal experiments were carried out following the guidelines of Yale University Institutional Animal Care and Use Committee (IACUC) with approved protocols (Chen 2020-20358; Chen 2021-20068; Lucas 2021-20375). This study does not involve human subjects.

Note that full information on the approval of the study protocol must also be provided in the manuscript.

Flow Cytometry

Plots

Confirm that:

☒ The axis labels state the marker and fluorochrome used (e.g. CD4-FITC).

☒ The axis scales are clearly visible. Include numbers along axes only for bottom left plot of group (a 'group' is an analysis of identical markers).

☒ All plots are contour plots with outliers or pseudocolor plots.

☒ A numerical value for number of cells or percentage (with statistics) is provided.

Methodology

Sample preparation	Various sample prep details are provided in the Methods section
Instrument	Flow cytometry data were collected on Attune focusing cytometer (Attune NxT Software v3.1) or BD FACSAria III Cell Sorter.
Software	FlowJo v.10.9.0 was used for flow cytometry data analysis.
Cell population abundance	No sorting was performed in this study. Lentivirus transduced cells were enriched using puromycin. Two days after transduction, stable B16 cell lines were established by puromycin selection at 10 µg/ml concentration and maintained in 2 µg/ml puromycin media.
Gating strategy	Cells were gated by FSC/SSC plot. To distinguish between positive and negative boundaries of the stained cells, negative control samples were analyzed and utilized as background.

☒ Tick this box to confirm that a figure exemplifying the gating strategy is provided in the Supplementary Information.